Estimation of solid-liquid interfacial potential enabled by quantitative analysis and relaxation observation of quadrupolar NMR

Maki, Hideshi
Tachibana, Takashi
Eun, Song Jung
Mizuhata, Minoru

(Citation)
Colloids and Surfaces A: Physicochemical and Engineering Aspects,604:125286

(Issue Date)
2020-11-05

(Resource Type)
journal article

(Version)
Accepted Manuscript

(URL)
https://hdl.handle.net/20.500.14094/90007532

Estimation of solid-liquid interfacial potential enabled by quantitative analysis and relaxation observation of quadrupolar NMR

Hideshi Maki[a,b,*], Takashi Tachibana[c], Song Jung Eun[b] and Minoru Mizuhata[b,d]

[a]Center for Environmental Management, Kobe University, 1-1 Rokkodai-cho, Nada-ku, Kobe 657-8501, Japan

[b]Department of Chemical Science and Engineering, Graduate School of Engineering, Kobe University, 1-1 Rokkodai-cho, Nada-ku, Kobe 657-8501, Japan

[c]Department of Chemical Science and Engineering, Faculty of Engineering, Kobe University, 1-1 Rokkodai-cho, Nada-ku, Kobe 657-8501, Japan

[d]Faculty of Chemistry, Jagiellonian University, Gronostajowa 2, 30-387 Kraków, Poland

CORRESPONDING AUTHOR FOOTNOTE

E-mail: maki@kobe-u.ac.jp

Keywords: qNMR; Quantitative NMR; ^{23}Na NMR; ^{35}Cl NMR; Zeta potential; Counterion condensation

ABSTRACT

Relaxation time measurements and quantitative analyses of quadrupolar nuclei via NMR were effective for the estimation of the interfacial potential at the solid-liquid interface. Moreover, quantitative nuclear magnetic resonance (qNMR) spectroscopy experiments for ^{23}Na and ^{35}Cl nuclei were performed. The calibration curve of the external standard aqueous NaCl solution showed excellent linearity over a considerably wide concentration range from 4×10^{-4} to 2 mol L^{-1} (an increase in concentration of 5000

times), with a simple experimental and analytical procedure. The relaxation time and detection rate of Cl^- ions in the ^{35}Cl NMR spectrum of a 0.10 mol L^{-1} NaCl(aq) solution with 10 vol% α-Al_2O_3 drastically decreased as the zeta potential of the solid phase (ζ_s) of α-Al_2O_3 approximated a negative value. Such a result was due to the decrease in both the mobility of Cl^- ions and the symmetry of the electrostatic field around ^{35}Cl nuclei caused by the electrostatic interactions between Cl^- ions and the solid surface. In the case of Na^+ ions, which have a charge opposite to that of Cl^- ions, the ζ_s dependences of the relaxation time and detection rate of Na^+ ions of ^{23}Na NMR were also opposite to those of ^{35}Cl NMR. Particularly, such values were almost constant when $\zeta_s > 0$ mV but decreased monotonically when $\zeta_s < 0$ mV. It was also clarified that the counterions condensed around the vicinity of the solid phase wherein the concentration of the counterions was approximately several tens of times higher than that in the bulk phase. The estimation of electrostatic field intensities not only at solid-liquid interfaces but also at liquid-liquid interfaces and various interfaces, including those in non-aqueous solvents, can thus be performed through the proposed method.

1. Introduction

The estimation of the interfacial potential at solid-liquid and liquid-liquid interfaces is important for understanding the various electrostatic interactions at the interfaces and the physicochemical phenomena resulting therefrom. Generally, the methods employed for the analysis of the interfacial potential include electroosmosis [1] and electrophoresis [1,2], as well as streaming potential [3,4], sedimentation potential [5,6], and ultrasonic vibration potential [7] methods. Although the values of the obtained interfacial potentials using such methods are similar, it is necessary to select an appropriate measurement method and the corresponding equipment depending on 1) the stability of a dispersion system, 2) the sizes of the primary particles and solute molecules, 3) the shape of the particles, 4) the permittivity of the solvent, etc. Furthermore, it is generally difficult to observe the interfacial potential at

the liquid-liquid interface in a solution system without solid particles as well as in a non-aqueous solvent system.

Nuclear magnetic resonance (NMR) has often been used to determine the structure of organic and inorganic compounds and to observe the dynamic behavior and interactions of molecules. From the viewpoint of NMR, atomic nuclei can be classified into two types: dipole nuclei, which have a spin quantum number of 1/2 (e.g., ^{1}H, ^{13}C, ^{19}F, ^{31}P), and quadrupole nuclei, which have spin quantum numbers other than 1/2 (e.g., ^{23}Na, ^{27}Al, ^{35}Cl, ^{81}Br) [8,9]. Dipole nuclei and quadrupole nuclei have fundamentally different factors in the NMR relaxation process. The NMR relaxation of dipole nuclei mainly depends on the mobility of molecules, which can be quantified using the rotational correlation time [10–13]. In contrast, a quadrupolar nucleus has a quadrupole moment because the electric charge distribution around the nucleus is not spherical but elliptical [14–18]. This quadrupole moment interacts with the electric field gradient caused by the asymmetry of the charge distribution around the observed nucleus. As a result, it remarkably promotes two NMR relaxations of the observed nucleus, namely [14–18]. Therefore, the NMR relaxation process of quadrupolar nuclei NMR strongly reflects the state of the electrostatic field around a nucleus; hence such a method is suitable for the observation of a local electric field.

NMR of quadrupolar nuclei can be applied to a wide range of cations and anions, including alkali metal ions and halide ions other than F^{-}, and has the following advantages inherent to NMR. (1) NMR is highly non-destructive. The radio pulse applied to a sample during NMR observation is low in energy, and the perturbation applied to an observed system is extremely small. (2) NMR can be observed throughout a wide range of ion concentrations (10^{-3}–10 mol L^{-1}) within a short time (approximately 10 min) without any pretreatment such as dilution or concentration. This advantage is due to the sensitivity of NMR, which has been improved in recent years by improving the S/N ratio of NMR probes and spectroscopic systems. (3) In addition to solution samples, samples with coexisting solid and liquid phases can be analyzed. Furthermore, a sample with a high solid fraction, and thus low fluidity, which would be difficult to analyze via electrophoresis or the streaming potential method, can be analyzed via

NMR. (4) Samples that contain non-aqueous solvents are also easy to analyze. Furthermore, samples that contain a solvent with low-permittivity are also easily analyzed. Because a high voltage is required to be applied to a low-permittivity solvent system, it is thus difficult to observe the zeta potential (ζ_s) by electro-osmosis, electrophoresis, or the streaming potential method. Utilizing the aforementioned advantages of NMR, we qualitatively evaluated the electrostatic effects of polyions using the electrostatic interaction between linear polycations and counterions by NMR experiments of alkali metals and halogens in a previous work [17–19]. According to Manning's ion-condensation theory, the strength of the electrostatic field of a polyion depends on the linear charge density of the polyion [20–22]. In fact, the dependence of the NMR relaxation rate of the counterion on the linear charge density was in good agreement with the theoretical prediction [17,18]. As such, we have determined that NMR of quadrupolar nuclei is effective for the evaluation of local electric fields, including those at liquid-liquid and solid-liquid interfaces.

The main purpose of this study was to observe the relationship between the NMR relaxation time and the signal intensities in ^{23}Na and ^{35}Cl NMR, which are NMR experiments for the quadrupolar nuclei of Na^+ and Cl^- ions, respectively, in a system with coexisting solid and liquid phases. Moreover, we aimed to determine the relationship between the NMR results and the ζ_s of the solid surface. To this end, dispersions of spherical SiO_2 or α-Al_2O_3 in NaCl aqueous solutions were prepared as solid-liquid systems, and the corresponding ^{23}Na and ^{35}Cl NMR analyses and NMR relaxation time measurements were carried out. If a clear correlation can be shown between the potential of the solid surface and the NMR signal intensities and relaxation times of ^{23}Na and ^{35}Cl nuclei, it can be expected to be applied as a probe to observe the electric fields of not only solid-liquid interfaces but also liquid-liquid interfaces. In addition, we evaluated the effect of the ζ_s of a solid on the electrostatic adsorption behavior of the counterions (Na^+ and Cl^-) on the solid surface in a solid-liquid system. There are many solid-liquid systems, such as battery materials, cosmetics, and foods. Within the vicinity of up to several tens of nanometers from the

surface of a solid phase, there is a unique region with physical properties that are significantly different from those in the bulk. Various heterogeneous coexistence field effects have been reported, such as changes in the complex structure of ions, changes in the activation energy of the electrical conductivity, changes in the ionic interactions between dissolved species, and lowering of the melting point of the liquid phase [11,23–27]. The findings of this study will also be useful for elucidating the influence of the electric field of a solid surface on the heterogeneous coexistence field effect of a solid-liquid system with a high solid fraction (e.g., slurries and pastes).

2. Experimental methods

2.1. Preparation of solid-liquid samples for zeta potential and all NMR measurements

All chemicals used in this work were of analytical grade. SiO_2 (KE-P50, NIPPON SHOKUBAI Co., Ltd., Japan) and α-Al_2O_3 (UA-5035, Showa Denko K.K., Japan) powders were used as the solid phase, and 0.10 mol L^{-1} NaCl(aq) solutions were used as the liquid phase. NaCl was dried at 500 °C for 4 h prior to the preparation of the solutions. The specific surface areas (S_W) of the SiO_2 and α-Al_2O_3 powders were determined from N_2 adsorption isotherms using the multipoint Brunauere-Emmette-Teller (BET) method (NOVA 2200e, Quantachrome Instruments Co., Ltd., Florida, USA), and the true densities were determined using Archimedes' principle. The main physical properties of the SiO_2 and α-Al_2O_3 powders are listed in Table S1. The SiO_2 or α-Al_2O_3 powders was adequately kneaded with the liquid phase and pH adjustment solutions (0.01 mol L^{-1} HCl + 0.10 mol L^{-1} NaCl aq. and 0.01 mol L^{-1} NaOH + 0.10 mol L^{-1} NaCl aq. for the measurement of ζ_s, and 0.01 mol L^{-1} HCl + 0.10 mol L^{-1} NaCl aq. and 0.01 mol L^{-1} KOH + 0.10 mol L^{-1} NaCl aq. for all NMR measurements) at predetermined solid/liquid ratios. The pH of the liquid phase was adjusted within the range of pH 2–11. The solid/liquid ratio was 0.01 wt% for the ζ_s measurements, and the volume fraction of the solid (ϕ_s) was 10 vol% for all NMR measurements. The volume fraction is defined by the following equation [11]:

$$\phi_S = \frac{V_S}{(V_L+V_S)} \quad (1)$$

where V_L and V_S are the volumes of the liquid and solid phases, respectively. In this work, the V_L and V_S values were determined using the following equations, respectively:

$$V_L = \frac{W_L}{\rho_L} \quad (2)$$

$$V_S = \frac{W_S}{\rho_S} \quad (3)$$

where W and ρ are the weight and true density of the sample, respectively.

2.2. ζ_s measurement

The ζ_s measurements on the surfaces of SiO_2 and α-Al_2O_3 nanoparticles in 0.10 mol L^{-1} NaCl(aq) solutions were recorded on an ELS-Z2000 (Otsuka Electronics Co., Ltd., Japan) using an electrophoretic light scattering method (laser Doppler method) at 25 ± 0.5 °C. When the electrolyte concentration is low and the thickness of the electrical double layer is sufficiently thin in comparison with the size of the particles, ζ_s can be determined using the Smoluchowski equation as follows:

$$\zeta_S = \frac{\eta U}{\varepsilon_0 \varepsilon} \quad (4)$$

where η is the viscosity of the solution, U is the electrophoretic mobility, ε_0 is the vacuum permittivity , and ε is the relative permittivity of the solution. The prepared solid-liquid samples were transferred to

quartz glass flow cells and stabilized at 25 ± 0.5 °C. The SiO_2 and α-Al_2O_3 nanoparticles were uniformly dispersed in the liquid phase throughout the ζ_s measurements. The determined ζ_s values are the averages of three measurements to minimize errors.

2.3. Quantitative NMR measurements of ^{23}Na and ^{35}Cl nuclei

All NMR spectra were recorded using a Varian INOVA 400 (9.39 T) pulse FT-NMR spectrometer with a tunable broadband probe at room temperature. To avoid the contamination of the sample solutions by D_2O which was used for the field-frequency locking, a coaxial NMR tube system was employed for all NMR measurements in this work. The coaxial NMR tube system consisted of borosilicate inner (516-I-5, Wilmad-LabGlass) and outer (516-CC-5, Wilmad-LabGlass) NMR tubes. A proper quantity of the measurement samples were put into the inner tube in the outer tube which a small amount of D_2O was put into as shown in Scheme S1. For the calibration curves of ^{23}Na and ^{35}Cl for quantitative NMR (qNMR) spectroscopy, NaCl was first dried at 500 °C for 4 h and dissolved in distilled water to prepare a 2 mol L^{-1} NaCl aqueous solution. Then, this solution was diluted to prepare a series of NaCl aqueous solutions with concentrations in the range of 0.4–2000 mmol L^{-1}. Sample tube spinning was stopped during all NMR measurements. The receiver gain of the radio frequency (RF) amplifier in the NMR spectrometer was set to a fixed value of 60 dB. All experiments were performed at 20 ± 0.5 °C.

For the ^{23}Na NMR experiments, all spectra were recorded at an operating frequency of 105.802 MHz, and a sweep width of 7450 kHz (190 ppm) was applied. The data acquisition time was 1.64 s, and the data during the free induction decay (FID) were collected at 20,000 points. A Lorentzian line-broadening factor of 2.0 Hz was applied to the total FID prior to Fourier transformation. The FID scans of 256–4000 times were recorded by applying a 0 s recycle delay between 90° pulse sequences with a pulse width of 18.2 μs to improve the signal-to-noise ratio and to avoid saturation. The ^{23}Na NMR

chemical shifts were determined against an external standard of 1 mol L^{-1} NaCl in 10% D_2O for the signal at 0 ppm.

In the case of the ^{35}Cl NMR experiments, all spectra were recorded at an operating frequency of 39.188 MHz, and a sweep width of 7840 Hz (200 ppm) was applied. The data acquisition time was 1.05 s, and the data during the FID were collected at 7,840 points. A Lorentzian line-broadening factor of 2.0 Hz was applied to the total FID prior to Fourier transformation. The FID scans of 256–4000 times were recorded by applying a 0 s recycle delay between 90° pulse sequences with a pulse width of 38.0 μs to improve the signal-to-noise ratio and to avoid saturation. The ^{35}Cl NMR chemical shifts were determined against an external standard of 1 mol L^{-1} NaCl in 10 % D_2O for the signal at 0 ppm. It was confirmed that further extension of the data acquisition time and the relaxation delay did not change the intensities of all ^{23}Na and ^{35}Cl NMR spectra. Furthermore, the S/N ratios of all ^{23}Na and ^{35}Cl NMR spectra were suitable for quantitative NMR signal analysis.

Careful phase and baseline corrections are necessary because errors in the phase and baseline of spectra result in inaccuracies in the integrated intensities of the NMR signals [11,28,29]. Thus, the NMR spectral data after the Fourier transform were corrected for the phase and baseline. Then, the integrated intensity was calculated manually by the sectional measurement method on Microsoft Excel using a frequency range that was five times the half height peak width of the signals.

2.4. NMR relaxation measurements for ^{23}Na and ^{35}Cl nuclei

The spin-lattice and spin-spin NMR relaxation times (T_1 and T_2, respectively) of all ^{23}Na and ^{35}Cl nuclei were determined by inversion recovery [30,31] and Carr-Purcell-Meiboom-Gill (CPMG) procedures, respectively [32,33]. Varian INOVA 400 (9.39 T) was used for the ^{23}Na and ^{35}Cl NMR relaxation measurements, as described in Section 2.3. All experiments were performed at 20 ± 0.5 °C. The theoretical spin-lattice and spin-spin NMR relaxation times of a nucleus are expressed by the following equations, respectively:

$$M_{(\tau)} = M_{(0)}\{1 - \exp(-\frac{\tau}{T_1})\} \quad (5)$$

$$M_{(\tau)} = M_{(0)} \cdot \exp(-\frac{\tau}{T_2}) \quad (6)$$

where $M_{(\tau)}$ is the *z*-magnetization after the pulse delay (τ) in the inversion recovery or CPMG procedure.

3. Results and discussions

3.1. Evaluation of experimental parameters affecting the accuracy and precision of ^{23}Na and ^{35}Cl qNMR

Many quantitative NMR analyses for dipole nuclei have already been reported [29,34–42]. In contrast, besides ^{27}Al qNMR, there have been few reports on NMR for quadrupolar nuclei, such as ^{23}Na and ^{35}Cl qNMR [28]. Therefore, careful evaluation is required for the development of ^{23}Na and ^{35}Cl qNMR. All ^{23}Na and ^{35}Cl qNMR evaluations were carried out using the integrated intensities of NMR signals due to the NaCl aqueous solutions. The qNMR spectra were analyzed using the following equation [11,28,29]:

$$\frac{N_{\mathrm{x}}}{N_{\mathrm{ref}}} = T \times 10^{\frac{Rg_{\mathrm{ref}} - Rg_{\mathrm{x}}}{20}} \times \frac{Ns_{\mathrm{ref}}}{Ns_{\mathrm{x}}} \times \frac{I_{\mathrm{x}}}{I_{\mathrm{ref}}} \quad (7)$$

where *N* is the concentration of the chemical species that produces the NMR signal, *Rg* is the receiver gain (in decibels) of the NMR spectrometer, *N*s is the number of FID scans, and *I* is the integrated intensity of the NMR signal. The subscripts “x” and “ref” correspond to the sample solution and the external reference of the NMR measurements, respectively. *T* indicates the specific constant value, which is affected by the conditions of the entire NMR observation system, including the NMR spectrometer, NMR probe, NMR sample tube, and is almost 1 when a similar NMR sample tube and the same NMR

equipment are used for all measurements. Therefore, the integrated intensity of the NMR signal should be approximately proportional to the number of nuclei giving rise to the NMR resonance.

To confirm the accuracy of the ^{23}Na and ^{35}Cl qNMR techniques, the influence of *N*s and *Rg* on the ^{23}Na and ^{35}Cl NMR signal intensities was evaluated, and the results are shown in Figs. S1(a), S1(b), S2(a), and S2(b). The extremely good linear relationships between the integrated intensities of the ^{23}Na and ^{35}Cl NMR signals and the *N*s and *Rg* values were confirmed. This result demonstrates the excellent reproducibility and accuracy of the pulse generator and radio frequency transmitter, as well as the linearity of the RF amplifier in the NMR equipment. Moreover, the influence of the FID acquisition time on the integrated intensity is shown in Figs. S1(c) and S2(c). The FID data cannot be fully obtained when the FID acquisition time is insufficiently short, and as a result, the integrated intensity decreases. However, the NMR measurement time increases when the FID acquisition time is excessively long; thus, an appropriate duration is desirable. In this study, the integrated intensities of the NMR signals were almost constant when the FID acquisition times were greater than 0.8 s for ^{23}Na NMR and 0.5 s for ^{35}Cl NMR. The aforementioned results thus show that it is possible to perform ^{23}Na and ^{35}Cl qNMR spectroscopy with high accuracy and within short measurement times.

The obtained ^{23}Na and ^{35}Cl NMR spectra consisted of unity singlet signals, which can be assigned to the free Na^+ and Cl^- ions. Figs. 1 and 2 show the relationship between the integrated intensities of the ^{23}Na and ^{35}Cl NMR signals per FID scan at *Rg* = 0 dB (the FID signals were not amplified by the RF amplifier circuit) and the concentrations of free Na^+ and Cl^- ions in the NaCl aqueous solutions with various concentrations. All the raw data of the integrated intensities of the ^{23}Na and ^{35}Cl NMR signals are listed in Tables S2 and S3 (Supporting Information), respectively. Theoretically, the proportional relationship between the integrated intensity of signal I_x and the number of nuclei, i.e., the concentration of chemical species C_x, is confirmed as follows [28]:

$$I_x = \text{slope} \times C_x \tag{8}$$

Taking the logarithm of both sides (i.e., log-log plot) allows us to verify the above relationship over a wide concentration range, as shown in Figs. 1(b) and 2(b). For example, if the concentration of the chemical species increases *x* times, the area intensity of the NMR signal also increases *x* times. Thus, theoretically, the slope (slope (log) in Table 1) of these log-log plots should be 1. The results of the linear approximation by the linear least squares method using the aforementioned relationships are shown in Table 1. There is extremely good linearity in the wide concentration range from 4×10^{-4} to 2 mol L^{-1} (an increase in the concentration of 5000 times) for both the real number axis plot (Figs. 1(a) and 2(a)) and the logarithmic axis plot (Figs. 1(b) and 2(b)). The equivalent concentration ranges for other spectroscopic methods (e.g., atomic absorption spectroscopy (AAS), inductively coupled plasma-optical emission spectrometry (ICP-OES), and UV-Vis spectroscopy) are narrow. Therefore, the extremely wide concentration range indicates that ^{23}Na and ^{35}Cl qNMR analyses are considerably useful.

3.2. Influence of the solid-state surface electric potential on ^{23}Na NMR relaxation and signal intensity

Fig. 3(a) shows the dependence of ζ_s on the pH of the 0.10 mol L^{-1} NaCl(aq) solutions with 0.01 wt% SiO_2 or α-Al_2O_3. It was confirmed that the point of zero charge (PZC) of SiO_2 and α-Al_2O_3 was at ca. 3 and 6, respectively. At a pH lower than the PZC, ζ_s is positive, and at a pH higher than the PZC, ζ_s is negative. Furthermore, the surface charge density of the solid phase (σ_s) was calculated using the following Grahame's equation based on the results of the ζ_s measurement [43,44], and the pH dependence of σ_s is shown in Fig. 3(b).

$$\sigma_s = \sqrt{8\varepsilon_0 \varepsilon I N_A z^2 k_B T} \sinh\left(\frac{ze\zeta_s}{2k_B T}\right) \quad (9)$$

In the above equation, ε_0 is the vacuum permittivity, ε is the permittivity of the solvent, I is the ionic strength of the solution, N_A is the Avogadro constant, Z is the valence of the counterion, k_B is the Boltzmann constant, T is the absolute temperature of the system, and e is the elementary charge. It can be confirmed that σ_s has the same pH dependency as the ζ_s potential.

In this study, the properties of the electrostatic interactions between the solid surfaces of SiO_2 and α-Al_2O_3 and the counterions Na+ and Cl^- were clarified using ^{23}Na and ^{35}Cl NMR. NMR chemical shifts are affected by electrons drifting around the nucleus in the bond directions and alterations in the electronic symmetry. In contrast, the NMR relaxation of a quadrupolar nucleus, such as ^{23}Na and ^{35}Cl, is determined mainly by the electric field gradient around the nucleus [14–18]. Therefore, quadrupolar nuclear NMR is extremely useful for observing the electrostatic interactions of quadrupolar ions. Fig. 4 shows the pH dependences of the ^{23}Na NMR spectra of 0.10 mol L^{-1} NaCl(aq) solutions with 10 vol% SiO_2 or α-Al_2O_3. For comparison, the NMR spectra of the 0.1 mol L^{-1} NaCl solution without any solid phase are also shown in Fig. 4. The chemical exchange rates between Na^+ ions with or without interactions with the solid surface are much faster than the time scale of NMR; hence, all ^{23}Na NMR signals are averaged, and the spectrum consists of a unity signal. While the ^{23}Na NMR chemical shift is largely independent of the pH of the solution, the linewidths of the signals are significantly pH-dependent. This increase in the linewidth is equivalent to a decrease in T_2 of the ^{23}Na nuclei and is attributed to a quadrupolar relaxation effect [15–17]. There are two factors that can contribute to an increase in the quadrupole relaxation time: the mobility of the nucleus and the symmetry of the electric field around a nucleus. A decrease in either of these factors can lead to a decrease in the relaxation time. The nuclei evaluated herein, with spin quantum numbers greater than 1/2 (^{23}Na and ^{35}Cl), possess nuclear quadrupolar moments. These nuclei are primarily relaxed by the interactions between such quadrupolar moments and the electric field gradients arising from the asymmetry of the surrounding electric charge distribution. The quadrupole spin-lattice and spin-spin relaxation time, T_{1Q} and T_{2Q}, of a quadrupolar

nucleus with spin quantum number, I_s, situated in a molecule with an isotropic correlation time, τ_c, and in the extreme narrowing region is defined as follows [14–18]:

$$\frac{1}{T_{1Q}} \approx \frac{1}{T_{2Q}} = \frac{3(2I_s+3)}{40{I_s}^2(2I_s-1)} \cdot \left(1+\frac{\eta^2}{3}\right) \cdot \left(\frac{e^2qQ}{h}\right)^2 \cdot \tau_c \qquad (10)$$

where Q is the quadrupole moment of the nucleus, q is the electric field gradient around the nucleus, η is the asymmetric parameter of the electric field gradient, and e and h are the electronic charge and Planck's constant, respectively. Furthermore, the NMR relaxation process of the quadrupole nucleus is predominated by the quadrupole relaxation process, and thus $T_1 \approx T_{1Q}$ and $T_2 \approx T_{2Q}$.

To quantitatively discuss the above relationship, the dependences of the T_1 and T_2 values of ^{23}Na NMR on the pH of the 0.10 mol L^{-1} NaCl(aq) solutions with or without 10 vol% SiO_2 or α-Al_2O_3 are shown in Fig. S3. Small T_1 and T_2 values correspond to a fast NMR relaxation rate, which indicates an increase in the electrostatic interactions between Na^+ ions and the solid surface. The following characteristics were observed for T_1 (Fig. S3(a)) and T_2 (Fig. S3(b)). In the pH region wherein ζ_s is positive (pH is 3 or less for SiO_2 and pH is 5 or less for α-Al_2O_3), T_1 and T_2 show almost constant maximum values. When ζ_s becomes negative due to an increase in pH, the asymmetry of the electric field gradient near the ^{23}Na nucleus (η in Eq. (10)) increases due to the electrostatic interactions between the negatively charged solid surface and Na^+ ions. Simultaneously, the mobility of Na^+ ions decreases (i.e., τ_c in Eq. (10) increases). As a result, T_1 and T_2 of ^{23}Na NMR begin to decrease. As ζ_s decreases further, the electrostatic interactions between the negatively charged solid surface and Na^+ ions increase, and thus T_1 and T_2 decrease. The decrease in T_1 and T_2 is more remarkable in the sample with SiO_2, which has a large ζ_s potential change. In contrast, the T_1 and T_2 values of the 0.10 mol L^{-1} NaCl(aq) solutions

without solid particles were almost constant regardless of the pH of the solution (× plots in Fig. S3) because there were no electrostatic interactions between the solid surface and Na^+ ions.

To further confirm the above discussion, the dependences of the T_1 and T_2 values of ^{23}Na NMR on the ζ_s of 0.10 mol L^{-1} NaCl(aq) solutions with 10 vol% SiO_2 or α-Al_2O_3 are shown in Fig. 5. Both T_1 and T_2 barely changed in the region wherein $\zeta_s > 0$ mV. In contrast, it was notable that T_1 and T_2 significantly decreased with a decrease in ζ_s in the region where $\zeta_s < 0$ mV. The latter result was due to the increasing electrostatic interactions between the solid surface and Na^+ ions. Unfortunately, the T_1 and T_2 values at the same ζ_s differed depending on whether SiO_2 or α-Al_2O_3 was used as the solid phase. Thus, ζ_s cannot be estimated exactly from the T_1 and T_2 values. The two following points are considered to be the main factors that contributed to the difference in the ζ_s dependences of T_1 and T_2 when the solid phase was either SiO_2 or α-Al_2O_3.

(1) There is a possibility that the difference in the solvent affinity of a material influences the mobility of Na+ ions through solvent molecules. If a standard sample of the same material is used, it may be possible to estimate the ζ_s value of the measured samples from the T_1 and T_2 values.
(2) The ζ_s values when ϕ_s = 10 vol% for the NMR measurements may be different from those when the concentration of the solid was 0.01 wt% for the ζ_s measurements.

In addition, T_2, which has a higher measurement accuracy, in principle, seems to be more suitable than T_1 for the estimation of ζ_s.

Based on the discussion in Section 3.1, the concentration of detected Na^+ ions by NMR can be determined from the ^{23}Na qNMR spectra of the 0.10 mol L^{-1} NaCl(aq) solutions with SiO_2 or α-Al_2O_3 using Fig. 1 (i.e., the relationship between the ^{23}Na NMR signal intensities and the concentration of free Na^+ ions). Furthermore, the detection rate of Na^+ ions by ^{23}Na qNMR (R_{Na+}) can be calculated as follows:

$$R_{Na^+} = \frac{N_{Na^+}}{C_{Na^+}} \quad (11)$$

where N_{Na^+} is the Na^+ ion concentration in the liquid phase (not including the volume of the solid phase) that is determined from the ^{23}Na qNMR signal intensity using Eq. (7), and C_{Na^+} is the total concentration of Na^+ ions in the liquid phase. Calculating the signal area intensity is generally easier than measuring T_1 and T_2. Consequently, if it is possible to approximate ζ_s from the NMR signal intensity, the estimated interfacial potentials at the solid-liquid interface and liquid-liquid interface would be significantly improved. Fig. 6(a) shows the dependence of R_{Na^+} on the pH of 0.10 mol L^{-1} NaCl(aq) solutions with or without 10 vol% SiO_2 or α-Al_2O_3. In the acidic region (pH < 6), almost all Na^+ ions in the liquid phase were detected by ^{23}Na NMR. In contrast, R_{Na^+} noticeably decreased with increasing pH in both 0.10 mol L^{-1} NaCl(aq) solutions with SiO_2 and α-Al_2O_3 in the basic region (pH > 6). When the ζ_s of the solid phase becomes negative due to an increase in pH, the mobility of the Na^+ ions that bind to the solid surface becomes extremely limited due to the electrostatic interactions between the negatively charged solid surface and the Na^+ ions. As a result, it is presumed that Na^+ ions with significantly reduced mobility cannot be detected by ^{23}Na NMR. It has been reported that in NaCl aqueous solutions, water molecules in the hydration sphere cannot be detected by ^1H NMR due to the extreme restriction of the mobility of these water molecules [45]. In this study, the same phenomenon was observed more clearly in the ^{23}Na qNMR, which is NMR spectroscopy for quadrupolar nuclei. Furthermore, to confirm the relationship between R_{Na^+} and the ζ_s of the solid phase, the dependence of R_{Na^+} on ζ_s is shown in Fig. 6(b). The correlation between R_{Na^+} and ζ_s was more clearly observed with the sample having α-Al_2O_3 than that with SiO_2 when either was used as the solid phase. In the case of the sample with the α-Al_2O_3 solid phase, R_{Na^+} is approximately 1 and is constant in the region wherein $\zeta_s > 0$ mV (Na^+ ions and the solid phase

surface do not interact electrostatically). However, in the region wherein $\zeta_s < 0$ mV, R_{Na+} monotonically decreases due to the electrostatic interactions between Na^+ ions and the solid phase surface. In contrast, in the case of the sample with the SiO_2 solid phase, R_{Na+} is approximately 1 and remains constant until the ζ_s reaches approximately –40 mV, at which point R_{Na+} rapidly decreases when $\zeta_s < -40$ mV. The difference in the dependences of R_{Na+} on ζ_s with either SiO_2 or α-Al_2O_3 is also considered to be due to (1) the difference in the solvent affinities of the solid materials and (2) the ζ_s dependency on the liquid phase fraction.

3.3. Influence of solid-state surface electric potential on ^{35}Cl NMR relaxation and signal intensity

The discussion in Section 3.2 revealed that T_1, T_2, and the signal intensity of ^{23}Na NMR spectra in this study are dominated by the electrostatic interactions between the solid surface and the counterions. Since Cl^- ions have a charge opposite to that of Na^+ ions, it is expected that the ^{35}Cl NMR results will show a pH dependence opposite to that of ^{23}Na NMR results. Fig. 7 shows the stack plot for the pH dependences of the ^{35}Cl NMR spectra of the 0.10 mol L^{-1} NaCl(aq) solutions with 10 vol% SiO_2 or α-Al_2O_3. For comparison, the NMR spectra of the 0.1 mol L^{-1} NaCl solution without any solid phase are also shown in Fig. 7. Similar to that in ^{23}Na NMR, the chemical exchange rates between Cl^- ions with and without interactions with the solid surface are much faster than the time scale of NMR. Hence, all ^{35}Cl NMR signals are averaged, and the spectrum consists of a unity signal. Moreover, the ^{35}Cl NMR chemical shift is largely independent of the pH of the solution. It should be noted that the pH dependence of the linewidth of the ^{35}Cl NMR signal is in contrast with that of ^{23}Na NMR. SiO_2 has a PZC of ca. 3, and the corresponding spectrum shows almost negative ζ_s values in the measured pH range of 1–11 in this study, as shown in Fig. 3(a). Hence, Cl^- ions barely interacted with the SiO_2 surface. In effect, the linewidths of the ^{35}Cl NMR signals of the 0.10 mol L^{-1} NaCl(aq) solutions with SiO_2 remained almost constant, and the linewidths were equivalent to those of the sample without SiO_2 as the solid phase. In

contrast, since α-Al_2O_3 has ζ_s values in the range of ± 10 mV, as shown in Fig. 3(a), the linewidths of the ^{35}Cl NMR signals of the 0.10 mol L^{-1} NaCl(aq) solutions with α-Al_2O_3 remarkably depended on the pH of the solutions. For the 0.10 mol L^{-1} NaCl(aq) solutions with α-Al_2O_3, the signal linewidths of the ^{23}Na NMR spectra notably increased with an increase in pH, as shown in Fig. 4, whereas those of the ^{35}Cl NMR spectra increased with decreasing pH, as shown in Fig. 7. This result is due to the opposite charges of Na^+ and Cl^- ions.

To discuss the above relationship quantitatively, the pH dependences of the T_1 and T_2 values of ^{35}Cl NMR using 0.10 mol L^{-1} NaCl(aq) solutions with SiO_2 or α-Al_2O_3 are shown in Fig. S4. As discussed in Section 3.2, the short T_1 and T_2 suggest increasing electrostatic interactions between Cl^- ions and the solid surface. The following pH dependences were observed for T_1 (Fig. S4(a)) and T_2 (Fig. S4(b)). Since SiO_2 had almost negative ζ_s values from pH 1 to 11, Cl^- ions barely interacted with the SiO_2 surface, and thus T_1 and T_2 were almost constant regardless of the pH of the 0.10 mol L^{-1} NaCl(aq) solution with SiO_2. In addition, such T_1 and T_2 values were slightly smaller than those of the NaCl(aq) solutions without any solid phase due to the decrease in Cl^-mobility caused by physical hindrances from the SiO_2 surface. In contrast, it was observed that T_1 and T_2 monotonically increased with increasing pH in the 0.10 mol L^{-1} NaCl(aq) solutions with α-Al_2O_3, which had ζ_s values in the range of ± 10 mV. This result strongly supports that the NMR relaxation process in this study was dominated by a decrease in the nuclear mobility and symmetry of the electric field around the nucleus, which was caused by the electrostatic interactions between the solid surface and the counterions, as discussed in Section 3.2.

To confirm the above interpretation, the dependences of the T_1 and T_2 values of ^{35}Cl NMR on the ζ_s of 0.10 mol L^{-1} NaCl(aq) solutions with 10 vol% SiO_2 or α-Al_2O_3 are shown in Fig. 8. The T_1 and T_2 values of the 0.10 mol L^{-1} NaCl(aq) solution with SiO_2, which had almost negative ζ_s values and Cl^- ions that barely interacted with the SiO_2 surface, are almost constant. This result is in contrast with the remarkable ζ_s dependence of the T_1 and T_2 values obtained via ^{23}Na NMR (Fig. 5). When the solid phase

was α-Al_2O_3, T_1 and T_2 decrease monotonically with increasing ζ_s. As the ζ_s of α-Al_2O_3 approximates a negative value, the interaction between Cl^- ions and the α-Al_2O_3 surface gradually increases, and T_1 and T_2 decrease because the mobility of the Cl^- ions and the symmetry of the electrostatic field around the ^{35}Cl nuclei decrease. Since the interaction between Cl^- ions and the α-Al_2O_3 surface can be considered to be an electrostatic factor, it is appropriate that the decrease in T_1 and T_2 should begin when $\zeta_s > 0$ mV.

The dependence of R_{Cl^-} on the pH of the 0.10 mol L^{-1} NaCl(aq) solutions with or without 10 vol% SiO_2 or α-Al_2O_3 is shown in Fig. 9(a). In contrast with the case of ^{23}Na NMR, in the pH region wherein the solid surface electric field becomes negative and the solid phase and Cl^- ions do not minimally interact (almost all pH ranges for SiO_2 and pH > 6 for α-Al_2O_3), almost all Cl^- ions existing in the liquid phase were detected by ^{35}Cl NMR. When the solid phase was SiO_2, R_{Cl^-} was almost constant at ca. 1.1. As such, approximately 10% more Cl^- ions were detected than the expected amount. This result clearly indicates that Cl^- counterions were transferred to the bulk phase from the vicinity of the SiO_2 surface because Na^+ ions were concentrated around the vicinity of the negatively charged SiO_2 surface. Although, electrical neutrality was maintained throughout the system. However, when the solid phase was α-Al_2O_3, in the range of pH < 6, in which range the surface electric field of α-Al_2O_3 was positive, R_{Cl^-} monotonically decreased with increasing ζ_s and decreasing pH. This result suggests that the mobility of Cl^- ions that were bound to the solid surface was extremely limited due to the electrostatic interactions between the solid surface and Cl^- ions. Thus, the Cl^- ions could not be detected by ^{35}Cl NMR. These results become clearer upon elucidating the dependence of R_{Cl^-} on the ζ_s of 0.10 mol L^{-1} NaCl(aq) solutions with SiO_2 or α-Al_2O_3, as shown in Fig. 9(b). When the solid phase was SiO_2, which mostly had negative ζ_s values at all pH values, R_{Cl^-} was virtually constant regardless of ζ_s. When the solid phase was α-Al_2O_3, the ζ_s dependence of R_{Cl^-} clearly shifts at approximately $\zeta_s = 0$ mV. Particularly, when $\zeta_s < 0$ mV, R_{Cl^-} is almost constant at ca. 1 because the Cl^- ions do not interact electrostatically with the

negatively charged α-Al_2O_3 surface. However, when $\zeta_s > 0$ mV, R_{Cl^-} monotonically decreases due to the electrostatic interactions between the positively charged α-Al_2O_3 surface and Cl^- ions.

3.4. Estimation of the local ion concentration within the vicinity of the solid surface

Finally, the local ion concentration within the vicinity of the solid surface was estimated. Assuming that the ions, which are undetectable by qNMR, strongly interact with the solid surface, as discussed above, the solid surface area per unit volume of the sample, *S*, and the amount of ions that are undetectable by qNMR per unit volume of the sample, *U*, are calculated as follows:

$$S = \phi_S \cdot \rho_S \cdot S_W \tag{12}$$

$$U = (1-R) \cdot (1-\phi_S) \cdot C \tag{13}$$

where *R* is R_{Na^+} or R_{Cl^-}, and *C* is the electrolyte concentration (0.10 mol L^{-1} in this study). Here, the distance affected by the electrostatic interactions between the solid surface and the ions is assumed to span from the solid surface to the thickness of the electric double layer (EDL). This distance is also called the Debye length (λ_D). As discussed above, the ions in the EDL interact strongly with the solid surface due to electrostatic interactions and thus cannot be detected by ^{23}Na and ^{35}Cl NMR. Therefore, the apparent concentration of Na^+ or Cl^- ions that are localized in the EDL, $C_{EDL,X}$ (X = Na^+ or Cl^-), is expressed as follows:

$$C_{EDL,X} \text{ (X = } Na^+ \text{ or } Cl^-\text{)} = \frac{U}{S \cdot \lambda_D} = \frac{(1-R) \cdot (1-\phi_S) \cdot C}{\phi_S \cdot \rho_S \cdot S_W \cdot \lambda_D} \tag{14}$$

Fig. 10 shows the dependences of C_{EDL,Na^+} (a) and C_{EDL,Cl^-} (b) on the ζ_s of 0.10 mol L^{-1} NaCl(aq) solutions with 10 vol% SiO_2 or αAl_2O_3. The condensation of Cl^- ions in the EDL could not be confirmed for the SiO_2 sample, which had a negative zeta potential at almost all pH values. Otherwise, $C_{EDL,X}$ (X = Na^+ or Cl^-) was found to reach a maximum of 20–40 mol L^{-1}. This simulation was carried out on the assumption that the distance affected by the electrostatic interactions due to the surface charge of the solid phase approximates the λ_D. Furthermore, it was expected that the actual $C_{EDL,X}$ (X = Na^+ or Cl^-) would be lower than the simulated concentration due to the diffusion of condensed counterions from the vicinity of the solid surface to the bulk phase. Nevertheless, it can still be concluded that the counterion, which has a concentration several tens of times higher than that in the bulk phase, condensed around the vicinity of the solid phase.

From the above discussion, this study showed that T_1, T_2, and qNMR signal intensities of quadrupolar nuclei are effective for the estimation of ζ_s on a solid surface. Moreover, the T_1, T_2, and qNMR of quadrupolar nuclei can be expected to be applied to the estimation of the electrostatic field intensities not only at solid-liquid interfaces but also at liquid-liquid interfaces, as well as various interfaces including those in non-aqueous solvents. Furthermore, C_{EDL,Na^+} when $\zeta_s > 0$ and C_{EDL,Cl^-} when $\zeta_s < 0$ had negative values. Some of these values may be analytical errors; however, it can be presumed that the major cause of such erroes is the remarkable transfer of counterions from the EDL to the bulk phase due to strong electrostatic repulsion.

4. Conclusions

The evaluation of solid-liquid interfacial potential was carried out using T_1 and T_2 measurements and the quantitative analysis of quadrupole nuclear NMR spectra, which strongly reflects the state of the electrostatic field around the nucleus. First, ^{23}Na and ^{35}Cl qNMR techniques were established. The effects of various experimental parameters, namely, the number of FID scans, receiver gain of the RF amplifier,

FID acquisition time, and the accuracy and precision of the ^{23}Na and ^{35}Cl qNMR techniques were carefully evaluated. The calibration curve of an external standard, NaCl(aq), showed excellent linearity over a wide concentration range from 4×10^{-4} to 2 mol L^{-1} (an increase in concentration of 5000 times). Furthermore, the experimental and analytical procedures were relatively simple.

As the ζ_s of α-Al_2O_3 approximated a positive value, the electrostatic interactions between Cl^- ions and the α-Al_2O_3 surface gradually increased, and thus the T_1 and T_2 values from the ^{35}Cl NMR experiments drastically decreased due to the decrease in mobility of the Cl^- ions and the symmetry of the electrostatic field around ^{35}Cl nuclei. In addition, the detection rate of Cl^- ions by ^{35}Cl NMR was almost constant at 1 when $\zeta_s < 0$ mV, whereas when $\zeta_s > 0$ mV, the detection rate decreased monotonically with decreasing Cl^- ion mobility due to the electrostatic interactions between Cl^- ions and the α-Al_2O_3 surface. In the case of Na^+ ions, which have a charge opposite to that of Cl^- ions, the ζ_s dependences of T_1, T_2, and the detection rate of Na^+ ions of ^{23}Na NMR were also opposite to those of ^{35}Cl NMR. In particular, such values were almost constant when $\zeta_s > 0$ mV but decreased monotonically when $\zeta_s < 0$ mV. Finally, it was clarified that the counterions that condensed around the vicinity of the solid phase had a concentration that was several tens of times greater than that in the bulk phase. The T_1, T_2, and qNMR of quadrupolar nuclei can be expected to be applied to the estimation of the electrostatic field intensities not only at solid-liquid interfaces but also at liquid-liquid interfaces, as well as various interfaces including those in non-aqueous solvents.

Acknowledgment

This work was supported by JSPS KAKENHI (Grant-in-Aid for Scientific Research(B)) Grant Number 20H02843.

Supplemental material

Table S1. Physical properties of SiO_2 (KE-P50, NIPPON SHOKUBAI Co., Ltd., Japan) and α-Al_2O_3 (UA-5035, Showa Denko K.K., Japan) powder.

Scheme S1. Coaxial NMR tube system to avoid the contamination of D_2O for field-frequency locking into the measurement samples.

Fig. S1. NMR measurement parameter dependences of the integrated intensities of ^{23}Na NMR signals due to free Na^+ ion in 1 mol L^{-1} NaCl aq. at 20 ± 0.5 ˚C. NMR measurement parameter: (a) number of FID scans, *N*s, (b) receiver gain of a RF amplifier, *Rg*, and (c) FID acquisition time. The integrated intensities for (b) and (c) are the values per FID scan, and for (a) and (c) are converted into the values before the input into the RF amplifier in an NMR spectrometer (i.e., *Rg* = 0 dB).

Fig. S2. NMR measurement parameter dependences of the integrated intensities of ^{35}Cl NMR signals due to free Cl^- ion in 1 mol L^{-1} NaCl aq. at 20 ± 0.5 ˚C. NMR measurement parameter: (a) number of FID scans, *N*s, (b) receiver gain of a RF amplifier, *Rg*, and (c) FID acquisition time. The integrated intensities for (b) and (c) are the values per FID scan, and for (a) and (c) are converted into the values before the input into the RF amplifier in an NMR spectrometer (i.e., *Rg* = 0 dB).

Table S2. All raw data for the relationships between the integrated intensities per FID scan (I_{freeNa}) of ^{23}Na NMR signals due to free Na^+ ion in *x* molL^{-1} NaCl aq. (*x* = ca. 1×10^{-3} – 2 mol L^{-1}) at 20 °C and the Na^+ ion concentrations (C_{freeNa}) as shown in Figs. 1(a) and 1(b). The I_{freeNa} values are converted into the values before the input into the RF amplifier in an NMR spectrometer (i.e., corresponding to *Rg* = 0 dB).

Table S3. All raw data for the relationships between the integrated intensities per FID scan (I_{freeCl}) of ^{35}Cl NMR signals due to free Cl^- ion in x molL^{-1} NaCl aq. (x = ca. 1×10^{-3} – 2 mol L^{-1}) at 20 °C and the Cl^- ion concentrations (C_{freeCl}) as shown in Figs. 2(a) and 1(b). The I_{freeCl} values are converted into the values before the input into the RF amplifier in an NMR spectrometer (i.e., corresponding to Rg = 0 dB).

Fig. S3. Dependences of the T_1 (a) and the T_2 (b) of ^{23}Na NMR on the pH of 0.10 mol L^{-1} NaCl aq. with or without 10 vol% SiO_2 or α-Al_2O_3.

Fig. S4. Dependences of the T_1 (a) and the T_2 (b) of ^{35}Cl NMR on the pH of 0.10 mol L^{-1} NaCl aq. with or without 10 vol% SiO_2 or α-Al_2O_3.

References

[1] S. Levine, G. H. Neale, The Prediction of Electrokinetic Phenomena within Multiparticle Systems I. Electrophoresis and Electroosmosis, J. Colloid Interface Sci. 47 (1974) 47 520–529.

[2] S. Levine, G. H. Neale, Electrophoretic mobility of multiparticle systems, J. Colloid Interface Sci. 49 (1974) 330–332.

[3] M. Smoluchowski, Handbuch der Elektrizität und des Magnetismus, Barth, Leipzig, 1921, pp. 399.

[4] R. F. Probstein, Physicochemical Hydrodynamics: An Introduction, 2nd ed., John Willy & Sons, New York, 1994.

[5] S. Levine, G. H. Neale, N. Epstein, The prediction of electrokinetic phenomena within multiparticle systems: II. Sedimentation potential, J. Colloid Interface Sci. 57 (1976) 424–437.

[6] B. J. Marlow, R. L. Rowell, Sedimentation Potential in Aqueous Electrolyte, Langmuir 1 (1985) 83–90.

[7] J. A. Enderby, On electrical effects due to sound waves in colloidal suspensions. Proc. Phys. Soc. 207A (1951) 329–342.

[8] S. Braun, H.-O. Kalinowski, S. Berger, 200 and More Basic NMR Experiments: A Practical Course, WILEY-VCH, Weinheim, 2004 (Chapter 9).

[9] R. K. Harris, NMR and the Periodic Table, Academic Press, New York, 1978.

[10] W. R. Carper, C. E. Keller, Direct determination of NMR correlation times from spinlattice and spin-spin relaxation times, J. Phys. Chem. A 101 (1997) 3246–3250.

[11] H. Maki, M. Takemoto, R. Sogawa, M. Mizuhata, Solvent molecule mobilities in propylene carbonate-based electrolyte solutions coexisting with fumed oxide nanoparticles, Colloid. Surface. A 562 (2019) 270–279.

[12] J. W. Akitt, NMR and Chemistry: An Introduction to Modern NMR Spectroscopy, 3rd ed., Chapman & Hall, London, 1992 (Chapter 4.2).

[13] I. Solomon, Relaxation processes in a system of two spins, Phys. Rev. 99 (1955) 559–565.

[14] J. W. Akitt, Multinuclear studies of aluminium compounds, Progress in NMR Spectroscopy 21 (1989) 1–149.

[15] A. Abragam, The Principles of Nuclear Magnetism, Clarendon Press, Oxford, 1961.

[16] J. W. Akitt, NMR and Chemistry: An Introduction to Modern NMR Spectroscopy, 3rd ed., Chapman & Hall, London, 1992 (Chapter 4.3).

[17] H. Maki, T. Miyajima, Linear Charge Density Dependence of the Polyelectrolyte Phase Volume of Ionic Dextran Sulfate as a Strong Acidic Polyion, Macromolecules 44 (2011) 5027–5035.

[18] H. Maki, K. Yoshida, H. Nariai, M. Mizuhata, Multinuclear NMR studies on the effect of electrostatic and hydrophobic interactions on bindings to counterions to weakly acidic and basic polyelectrolytes, Colloid. Surface. A 471 (2015) 1–10.

[19] H. Maki, K. Ibaragi, Y. Fujimoto, H. Nariai, M. Mizuhata, Transitions from simple electrolyte to polyelectrolyte in a series of polyphosphates, Colloid. Surface. A 484 (2015) 153–163.

[20] G. S. Manning, Counterion binding in polyelectrolyte theory, Acc. Chem. Res. 12 (1979) 443–449.

[21] G. S. Manning, Limiting laws and counterion condensation in polyelectrolytesolutions I. Colligative properties, J. Chem. Phys. 51 (1969) 924–933.

[22] G. S. Manning, The molecular theory of polyelectrolyte solutions with applications to the electrostatic properties of polynucleotides, Rev. Biophys. 11 (1978) 179–246.

[23] M. Mizuhata, H. Ikeda, A. Kajinami, S. Deki, Effect of solid surface on vibrational modes of solution in solid/liquid hetero-phase system, J. Mol. Liq. 83 (1999) 179–189.

[24] A. B. Béléké, M. Mizuhata, S. Deki, Anomalous properties of molten alkali nitrates coexisting with aluminum oxides by hetero-phase effect, Spectroscopy 40 (2006) 66–79.

[25] S. Deki, S. Nakamura, A. Kajinami, Y. Kanaji, M. Mizuhata, Properties of $CaCl_2$ hydrate with an inorganic powder. Part 1.—Electrical conductivity of $CaCl_2 \cdot nH_2O$ (n= 6.00–7.35) with α-Al_2O_3 powder, J. Chem. Soc. Faraday Trans. 89 (1993) 3805–3810.

[26] S. Deki, A. Kajinami, Y. Kanaji, M. Mizuhata, K. Nagata, Properties of $CaCl_2$ hydrate with an inorganic powder. Part 2.—Melting behaviour and thermodynamic properties of $CaCl_2 \cdot nH_2O$ (n= 6.00–7.35) with α-Al_2O_3 or α-SiC powder, J. Chem. Soc. Faraday Trans. 89 (1993) 3811–3815.

[27] S. Deki, M. Mizuhata, S. Rakuno, A. Kajinami, Electrical conductivity of solid/liquid coexisting systems: dependence of electrical conductivity on surface hydrophilicity, J. Colloid Interface Sci. 168 (1994) 198–205.

[28] H. Maki, G. Sakata, M. Mizuhata, Quantitative NMR of quadrupolar nucleus as a novel analytical method : Hydrolysis behavior analysis of aluminum ion, Analyst 142 (2017) 1790–1799.

[29] H. Maki, Y. Okumura, H. Ikuta, M. Mizuhata, Ionic Equilibria for Synthesis of TiO_2 Thin Films by the Liquid Phase Deposition, J. Phys. Chem. C 118 (2014) 11964–11974.

[30] R. L. Vold, J. S. Waugh, M. P. Klein, D. E. Phelps, Measurement of spin relaxation in complex systems, J. Chem. Phys. 48 (1968) 3831–3832.

[31] S. Braun, H.-O. Kalinowski, S. Berger, 200 and More Basic NMR Experiments: A Practical Course, WILEY-VCH, Weinheim, 2004 (Chapter 6.1).

[32] S. Meiboom, D. Gill, Modified spin-echo method for measuring nuclear relaxation times, Rev. Sci. Instrum. 29 (1958) 688–691.

[33] S. Braun, H.-O. Kalinowski, S. Berger, 200 and More Basic NMR Experiments: A Practical Course, WILEY-VCH, Weinheim, 2004 (Chapter 6.2).

[34] G. F. Pauli, B. U. Jaki, D. C. Lankin, Quantitative ^{1}H NMR: Development and Potential of a Method for Natural Products Analysis, J. Nat. Prod. 68 (2005) 133–149.

[35] F. Malz, H. J. Jancke, Validation of quantitative NMR, Pharm. Biomed. Anal. 38 (2005) 813–823.

[36] U. Brinkmann-Trettenes, P. C. Stein, B. Klösgen, A. J. Bauer-Brandl, A method for simultaneous quantification of phospholipid species by routine ^{31}P NMR. Pharmaceut, Biomed. 70 (2012) 708–712.

[37] E. Szłyk, P. Hrynczyszyn, Phosphate additives determination in meat products by 31-phosphorus nuclear magnetic resonance using new internal reference standard: Hexamethylphosphoroamide, Talanta 84 (2011) 199–203.

[38] D. S. Argyropoulos, H. Li, A. R. Gaspar, K. Smith, L. A. Lucia, O. J. Rojas, Quantitative ^{31}P NMR detection of oxygen-centered and carbon-centered radical species, Bioorg. Med. Chem. 14 (2006) 4017–4028.

[39] S. K. Bharti, R. Roy, Quantitative ^{1}H NMR spectroscopy, Trends Anal. Chem. 35 (2012) 5–26.

[40] G. F. Pauli, T. Gödecke, B. U. Jaki, D. C. Lankin, Quantitative ^{1}H NMR. Development and Potential of an Analytical Method: An Update, J. Nat. Prod. 75 (2012) 834–851.

[41] N. M. Do, M. A. Olivier, J. J. Salisbury, C. B. Wager, Application of Quantitative ^{19}F and ^{1}H NMR for Reaction Monitoring and In Situ Yield Determinations for an Early Stage Pharmaceutical Candidate, Anal. Chem. 83 (2011) 8766–8771.

[42] P. Giraudeau, I. Tea, G. S. Remaud, S. Akoka, Reference and normalization methods: Essential tools for the intercomparison of NMR spectra, J. Pharmaceut. Biomed. 93 (2014) 3–16

[43] D. C. Grahame, Diffuse Double Layer Theory for Electrolytes of Unsymmetrical Valence Types, J. Chem. Phys. 21 (1953) 1054–1060.

[44] J. Seo, J. H. Kim, M. Lee, J. Moon, D. K. Yi, U. Paik, Size-dependent interactions of silica nanoparticles with a flat silica surface, J. Colloid Interface Sci. 483 (2016) 177–184.

[45] H. Maki, R. Sogawa, M. Fukui, S. Deki, M. Mizuhata, Quantitative Analysis of Water Activity Related to Hydration Structure in Highly Concentrated Aqueous Electrolyte Solutions, Electrochemistry 87 (2019) 139–141.

Tables

Table 1. Fitting parameters of the linear approximating for the relationships between the integrated intensities per FID scan (I_{free}) of ^{23}Na and ^{35}Cl NMR signals due to free Na^+ and Cl^- ions in x mol L^{-1} NaCl aq. (x = ca. 1×10^{-3} – 2 mol L^{-1}) at 20 °C and the Na^+ and Cl^- ion concentrations as shown in Fig. 1(a) and 1(b).

(a) Linearly approximating for the real number axis plot ((i.e., Figs. 1(a) and 2(a)) by Eq. (8).

	Slope	Intercept	Correlation coefficient
^{23}Na qNMR	3.022×10^2	1.6984×10^3	0.99951
^{35}Cl qNMR	1.4385×10^2	-3.637×10^2	0.99990

(b) Linearly approximating for the logarithmic axis plot ((i.e., Figs. 1(b) and 2(b)).

	Slope	Intercept	Correlation coefficient
^{23}Na qNMR	1.0018	2.486	0.99992
^{35}Cl qNMR	1.0033	1.1427	0.99994

Figure captions

Fig. 1. Relationships between the integrated intensity per FID scan (I_{freeNa}) of ^{23}Na NMR signals and the concentration of free Na^+ ion in x mol L^{-1} NaCl aq. (x = ca. 0.4 – 2000 mmol L^{-1}) at 20 ± 0.5 ˚C. (a) double linear chart, (b) double logarithmic chart. Solid lines refer to the calculated straight lines by the use of pertinent parameters in Table 1 obtained by the linear approximation. The I_{freeNa} values are converted into the values before the input into the RF amplifier in an NMR spectrometer (i.e., corresponding to the receiver gain of 0 dB). All raw data are listed in Table S2.

Fig. 2. Relationships between the integrated intensity per FID scan (I_{freeCl}) of ^{35}Cl NMR signals and the concentration of free Cl^- ion in x mol L^{-1} NaCl aq. (x = ca. 0.4 – 2000 mmol L^{-1}) at 20 ± 0.5 ˚C. (a) double linear chart, (b) double logarithmic chart. Solid lines refer to the calculated straight lines by the use of pertinent parameters in Table 1 obtained by the linear approximation. The I_{freeCl} values are converted into the values before the input into the RF amplifier in an NMR spectrometer (i.e., corresponding to the receiver gain of 0 dB). All raw data are listed in Table S3.

Fig. 3. Dependences of the ζ_s (a) and the σ_S (b) on the pH of 0.10 mol L^{-1} NaCl aq. with 0.01 wt% SiO_2 or α-Al_2O_3. The pH control was carried out by 0.01 mol L^{-1} HCl or NaOH aq. The σ_S were calculated by Eq. (10) from the ζ_s.

Fig. 4. Stack plot for the pH dependence of ^{23}Na NMR spectra of 0.10 mol L^{-1} NaCl aq. with 10 vol% SiO_2 or α-Al_2O_3.

Fig. 5. Dependences of the T_1 (a) and the T_2 (b) of ^{23}Na NMR on the ζ_s of 0.10 mol L^{-1} NaCl aq. with 10 vol% SiO_2 or α-Al_2O_3.

Fig. 6. Dependences of the R_{Na+} on the pH (a) and the ζ_s (b) of 0.10 mol L^{-1} NaCl aq. with or without 10 vol% SiO_2 or α-Al_2O_3. The R_{Na+} are the detection rate which were calculated from the integrated intensities of the ^{23}Na qNMR signal by Eq. (12).

Fig. 7. Stack plot for the pH dependence of ^{35}Cl NMR spectra of 0.10 mol L^{-1} NaCl aq. with 10 vol% SiO_2 or α-Al_2O_3.

Fig. 8. Dependences of the T_1 (a) and the T_2 (b) of ^{35}Cl NMR on the ζ_s of 0.10 mol L^{-1} NaCl aq. with 10 vol% SiO_2 or α-Al_2O_3.

Fig. 9. Dependences of the R_{Cl^-} on the pH (a) and the ζ_s (b) of 0.10 mol L^{-1} NaCl aq. with or without 10 vol% SiO_2 or α-Al_2O_3. The R_{Cl^-} are the detection rate which were calculated from the integrated intensities of the ^{35}Cl qNMR signal by Eq. (12).

Fig. 10 Dependences of the $C_{EDL,Na+}$ (a) and C_{EDL,Cl^-} (b) on the ζ_s of 0.10 mol L^{-1} NaCl aq. with 10 vol% SiO_2 or α-Al_2O_3. The $C_{EDL,Na+}$ and C_{EDL,Cl^-} are the apparent concentrations of Na^+ and Cl^- ions in an electric double layer (EDL) of a solid phase which were calculated from Eq. (15).

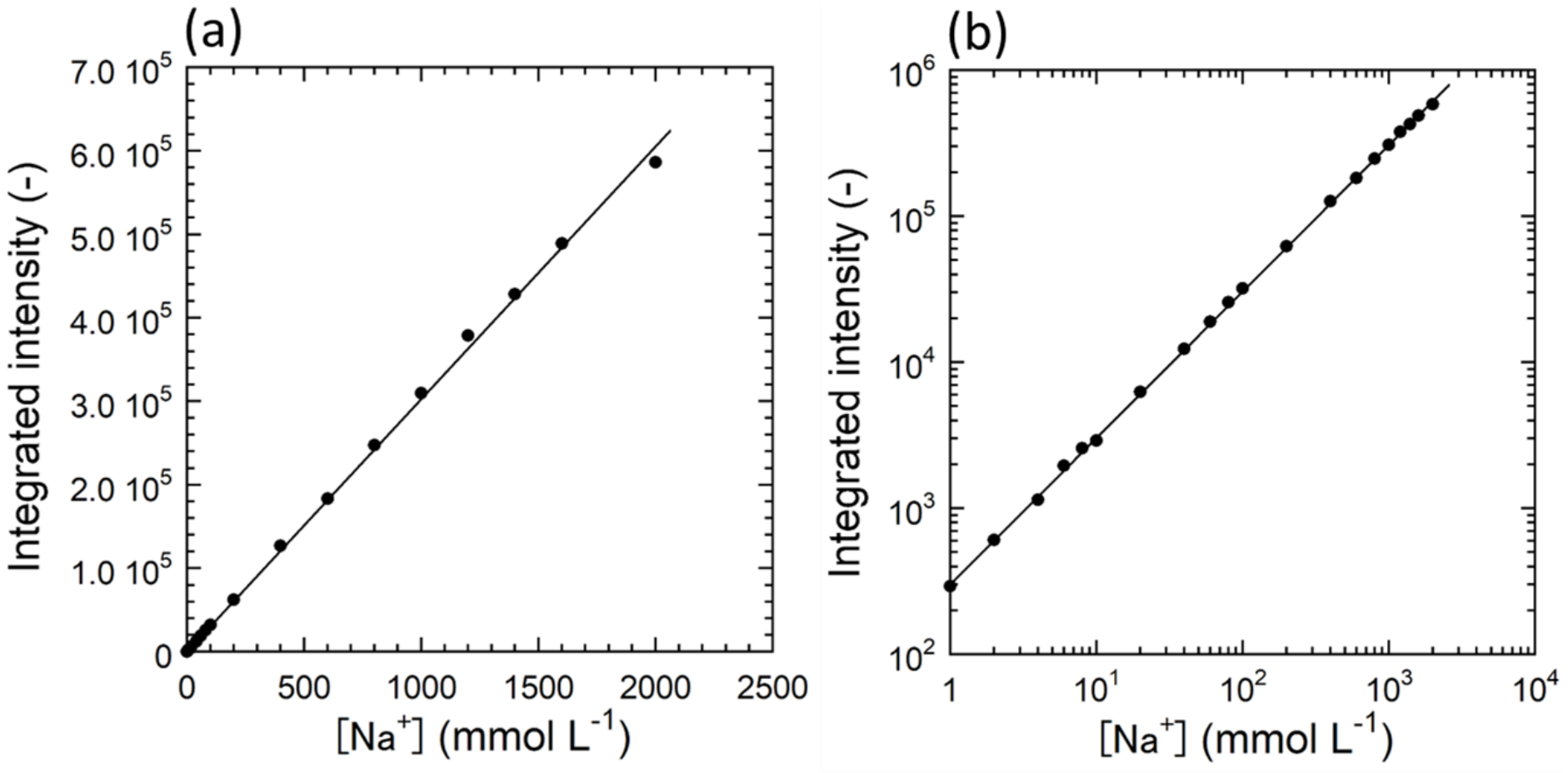

Figure 1. Relationships between the integrated intensity per FID scan (I_{freeNa}) of ^{23}Na NMR signals and the concentration of free Na^+ ion in *x* mol L^{-1} NaCl aq. (*x* = ca. 0.4 – 2000 mmol L^{-1}) at 20 ± 0.5 ˚C. (a) double linear chart, (b) double logarithmic chart. Solid lines refer to the calculated straight lines by the use of pertinent parameters in Table 1 obtained by the linear approximation. The I_{freeNa} values are converted into the values before the input into the RF amplifier in an NMR spectrometer (i.e., corresponding to the receiver gain of 0 dB). All raw data are listed in Table S2.

Figure 1

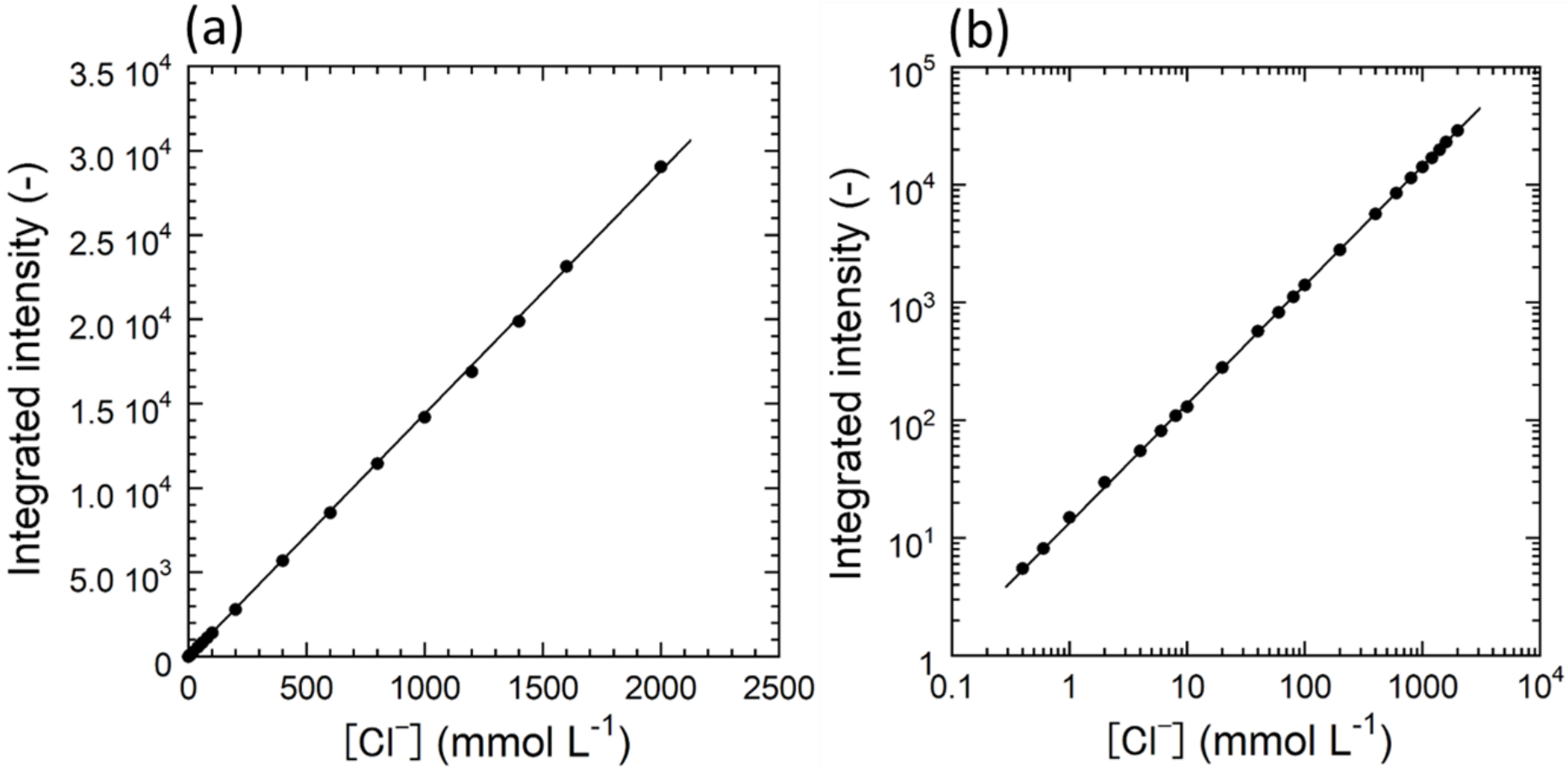

Figure 2. Relationships between the integrated intensity per FID scan (I_{freeCl}) of ^{35}Cl NMR signals and the concentration of free Cl^- ion in *x* mol L^{-1} NaCl aq. (*x* = ca. 0.4 – 2000 mmol L^{-1}) at 20 ± 0.5 ˚C. (a) double linear chart, (b) double logarithmic chart. Solid lines refer to the calculated straight lines by the use of pertinent parameters in Table 1 obtained by the linear approximation. The I_{freeCl} values are converted into the values before the input into the RF amplifier in an NMR spectrometer (i.e., corresponding to the receiver gain of 0 dB). All raw data are listed in Table S3.

Figure 2

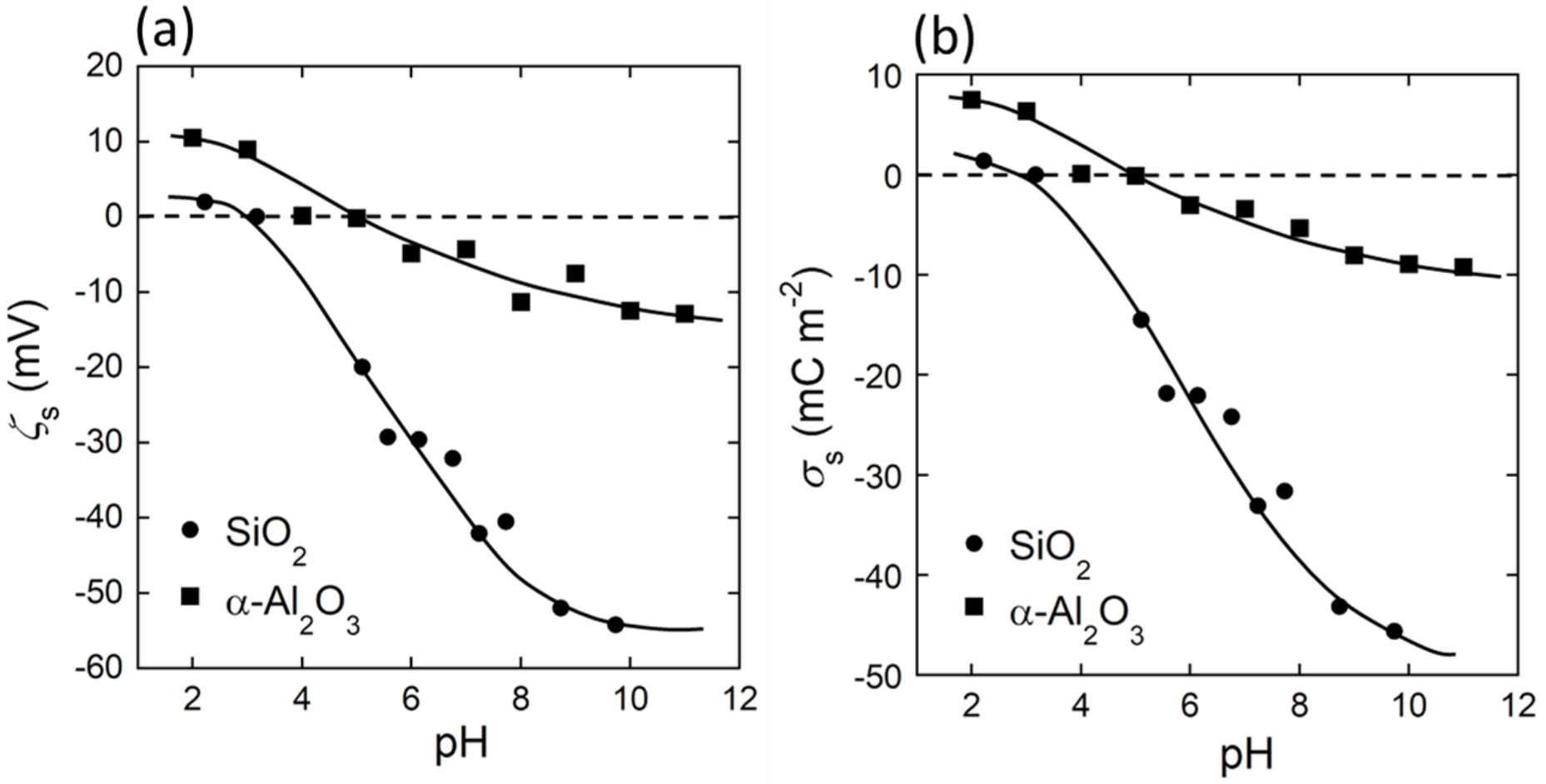

Figure 3. Dependences of the ζ_s (a) and the σ_S (b) on the pH of 0.10 mol L^{-1} NaCl aq. with 0.01 wt% SiO_2 or a-Al_2O_3. The pH control was carried out by 0.01 mol L^{-1} HCl or NaOH aq. The σ_S were calculated by eq 9 from the ζ_s.

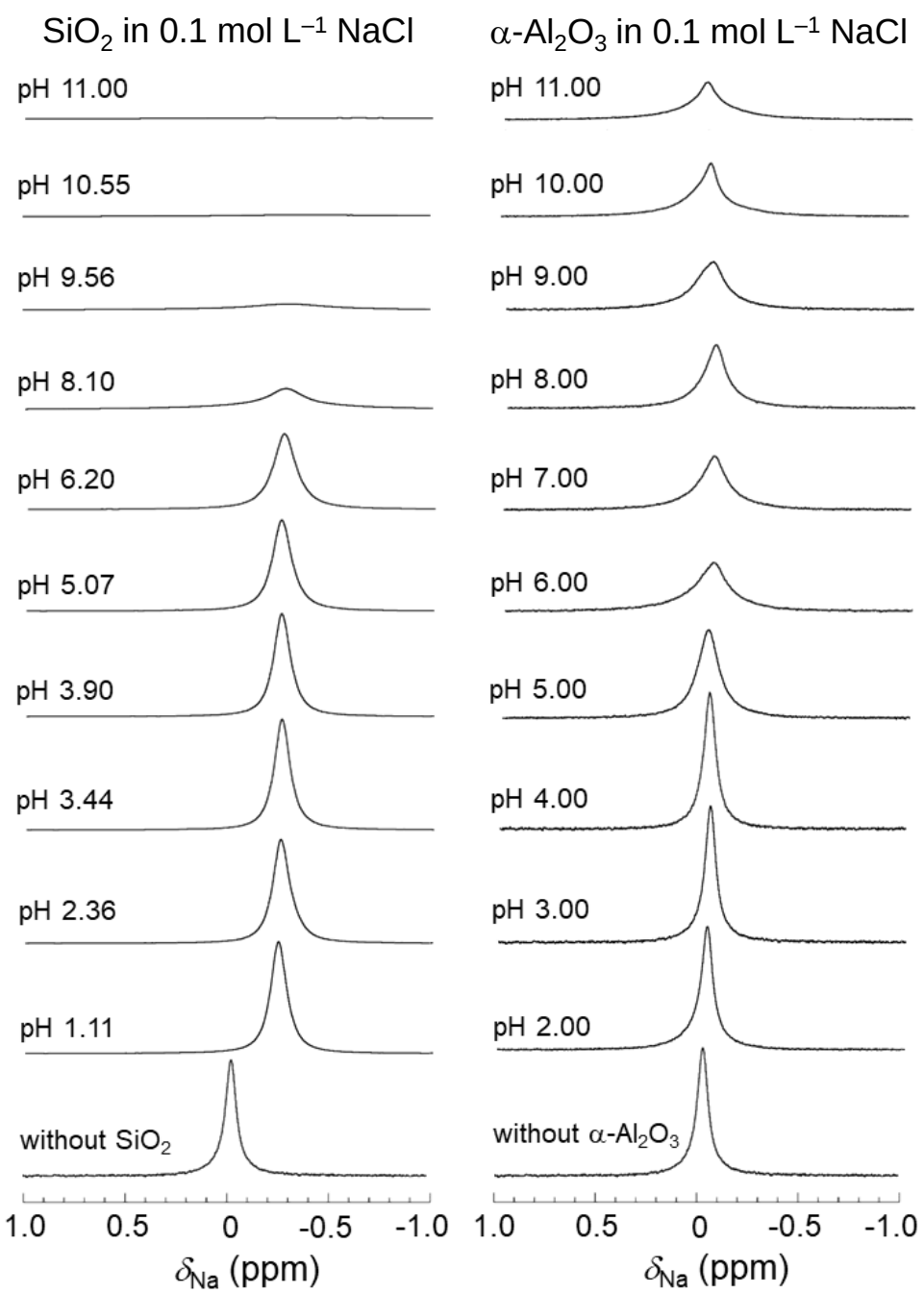

Figure 4. Stack plot for the pH dependence of ^{23}Na NMR spectra of 0.10 mol L^{-1} NaCl aq. with 10 vol% SiO_2 or α-Al_2O_3.

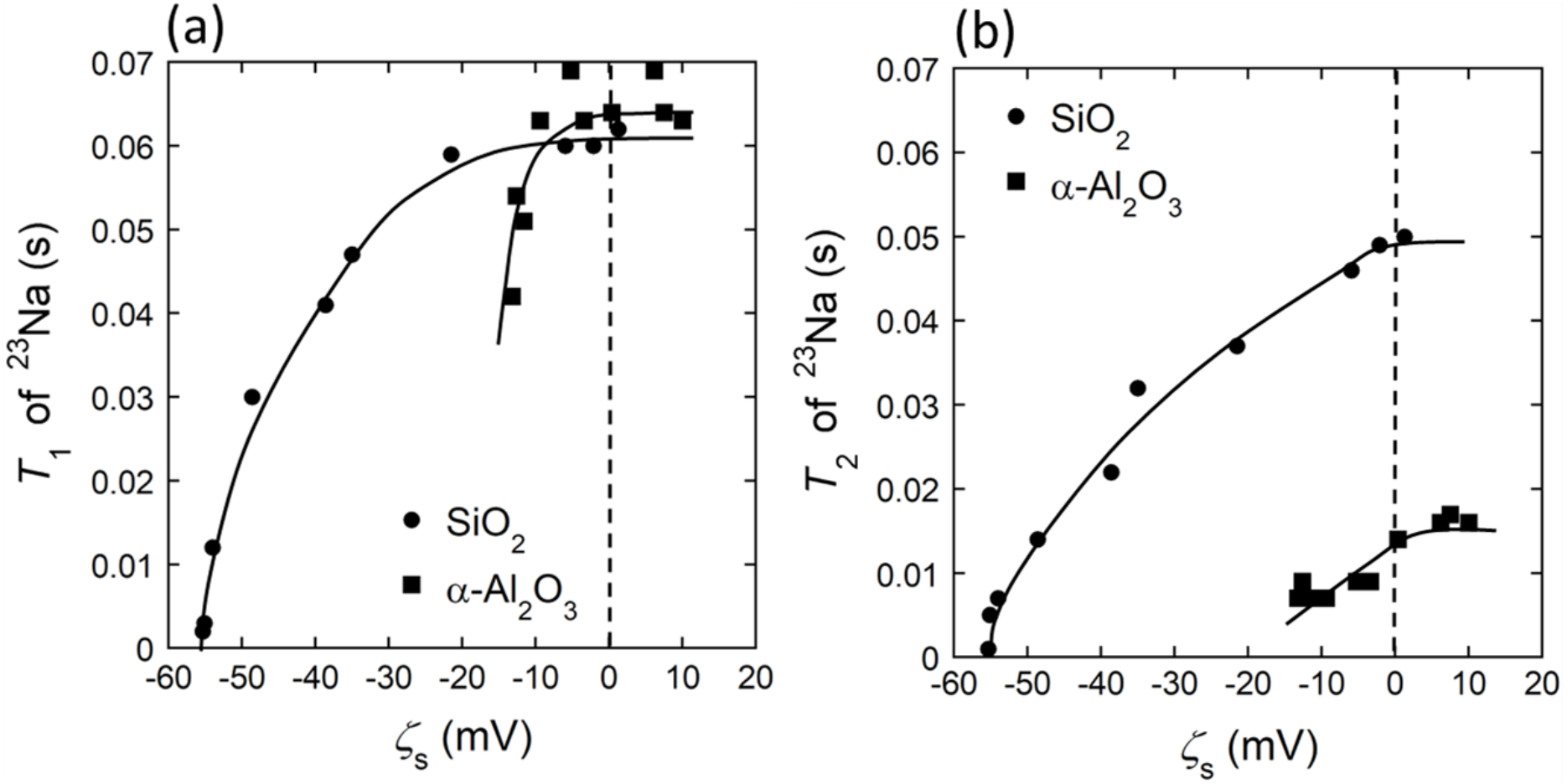

Figure 5. Dependences of the T_1 (a) and the T_2 (b) of ^{23}Na NMR on the ζ_s of 0.10 mol L^{-1} NaCl aq. with 10 vol% SiO_2 or α-Al_2O_3.

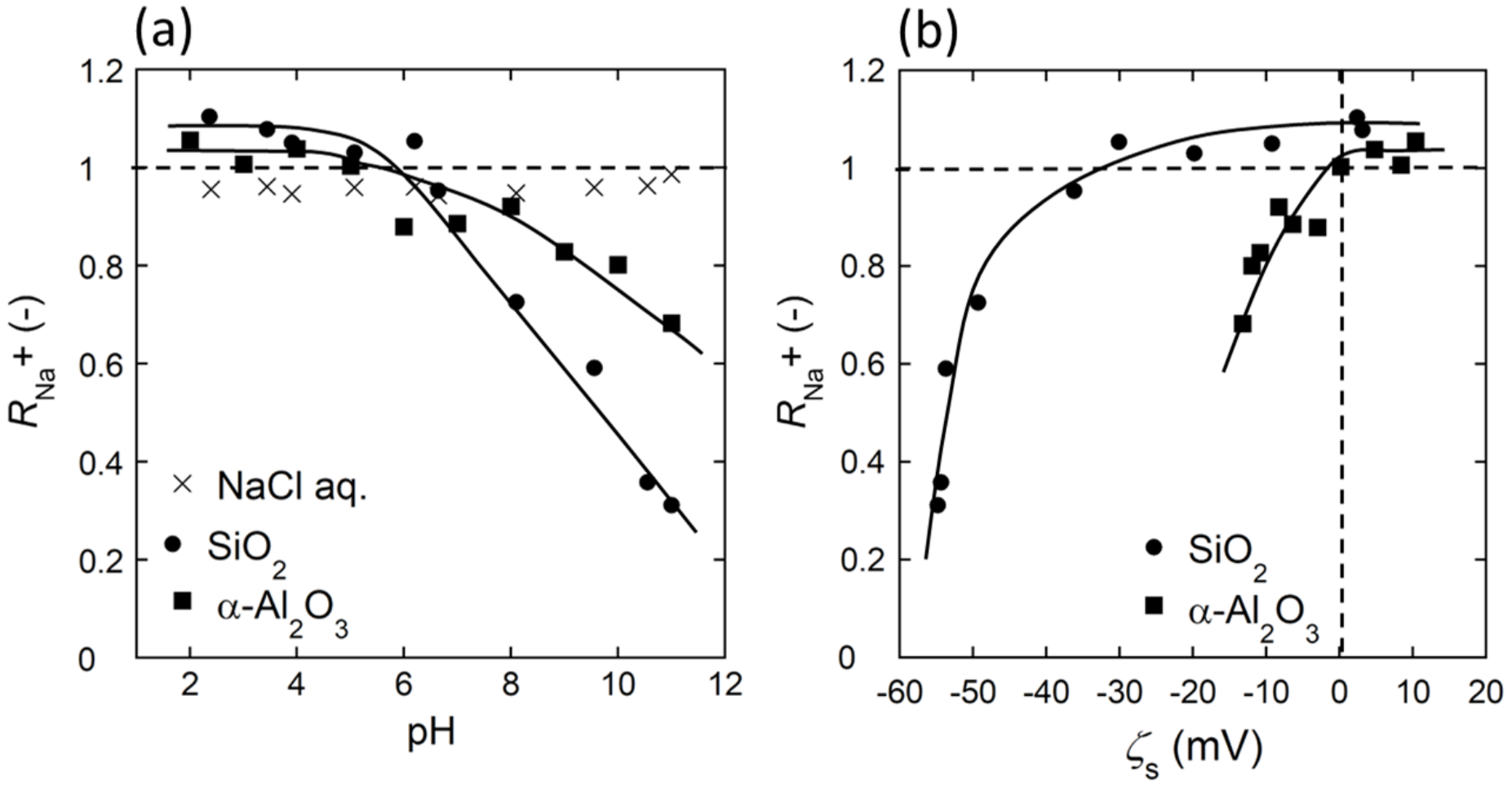

Figure 6. Dependences of the R_{Na}+ on the pH (a) and the ζ_s (b) of 0.10 mol L^{-1} NaCl aq. with or without 10 vol% SiO_2 or α-Al_2O_3. The R_{Na}+ are the detection rate which were calculated from the integrated intensities of the ^{23}Na qNMR signal by eq 11.

Figure 6

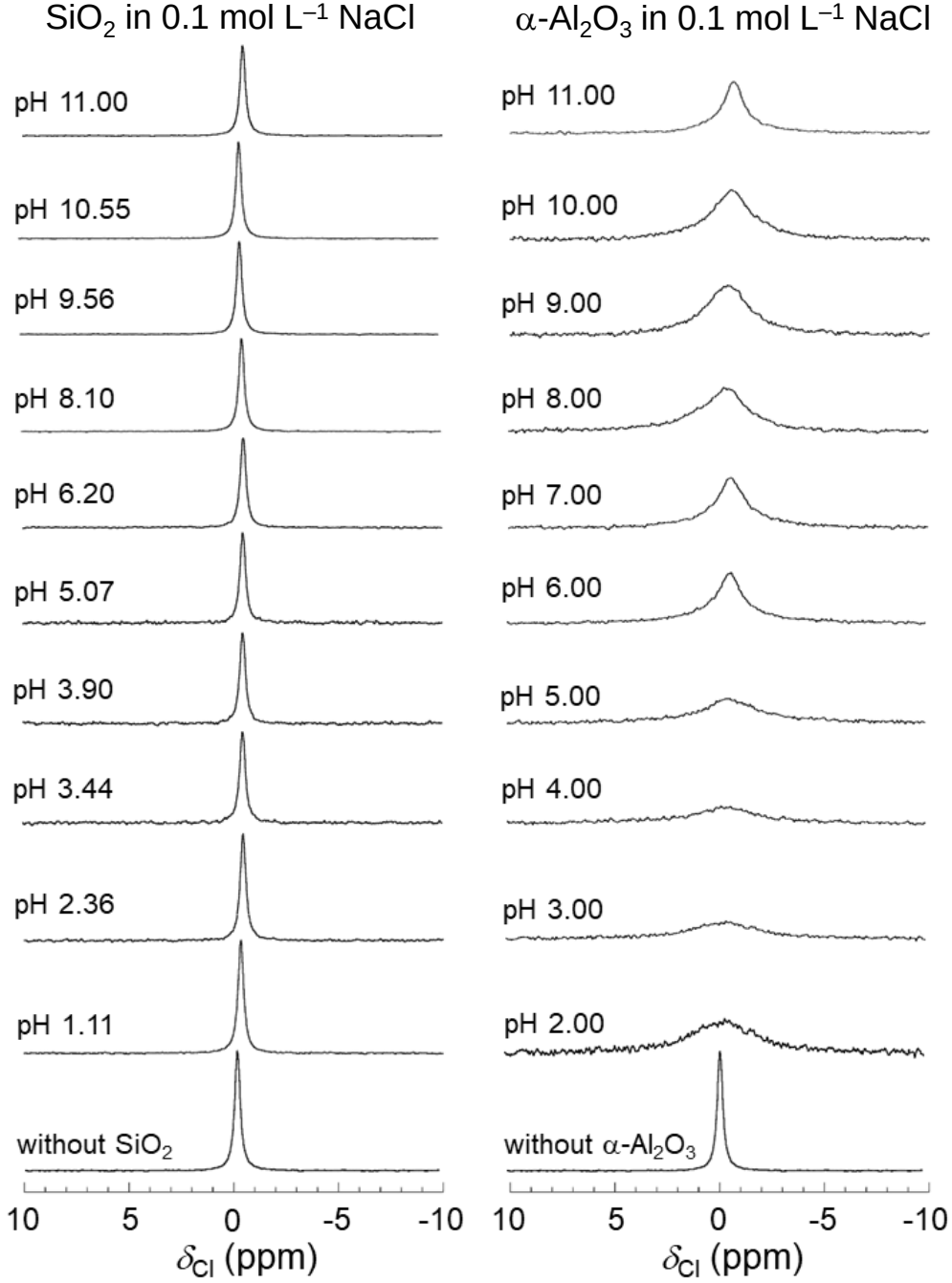

Figure 7. Stack plot for the pH dependence of ^{35}Cl NMR spectra of 0.10 mol L^{-1} NaCl aq. with 10 vol% SiO_2 or α-Al_2O_3.

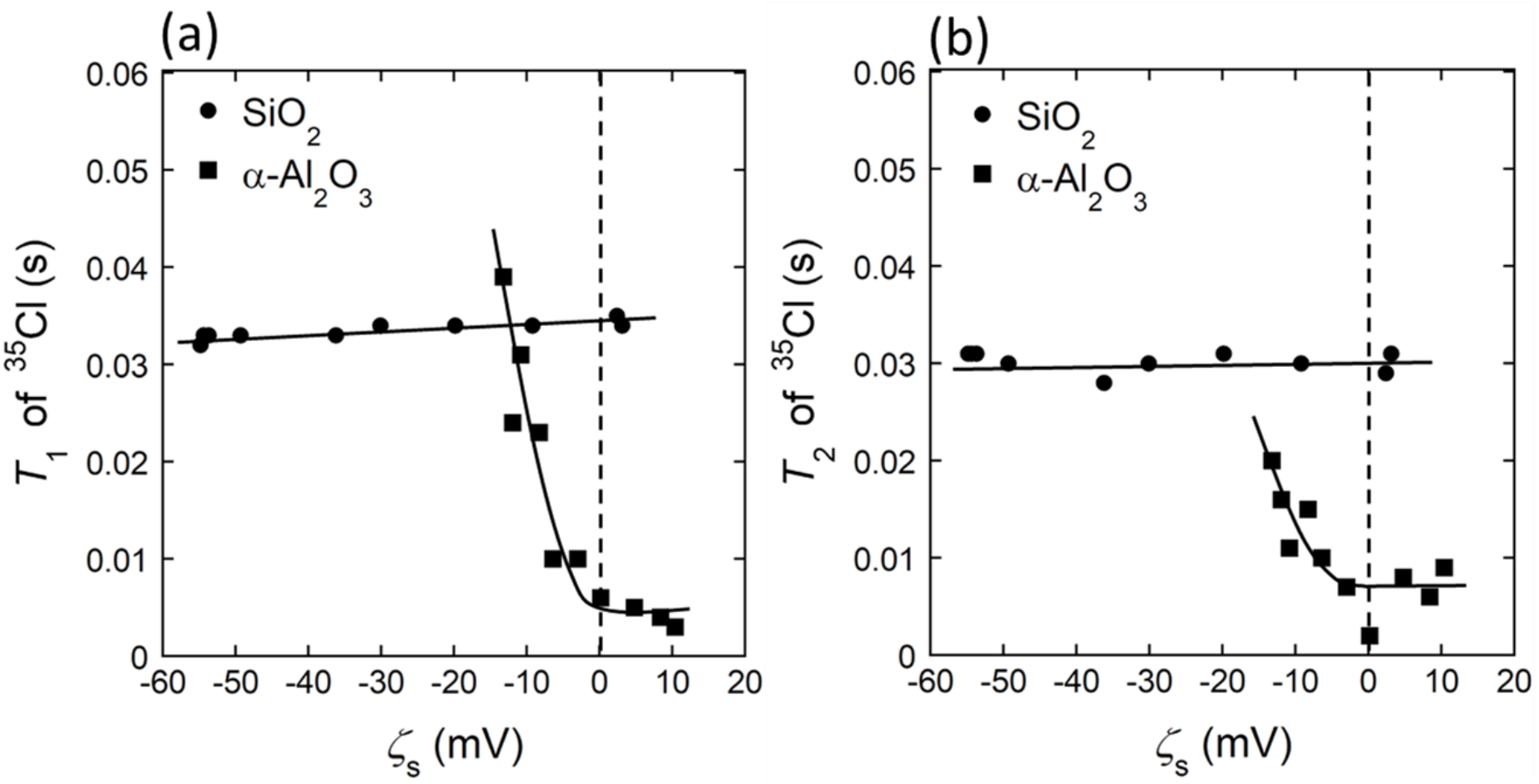

Figure 8. Dependences of the T_1 (a) and the T_2 (b) of ^{35}Cl NMR on the ζ_s of 0.10 mol L^{-1} NaCl aq. with 10 vol% SiO_2 or a-Al_2O_3.

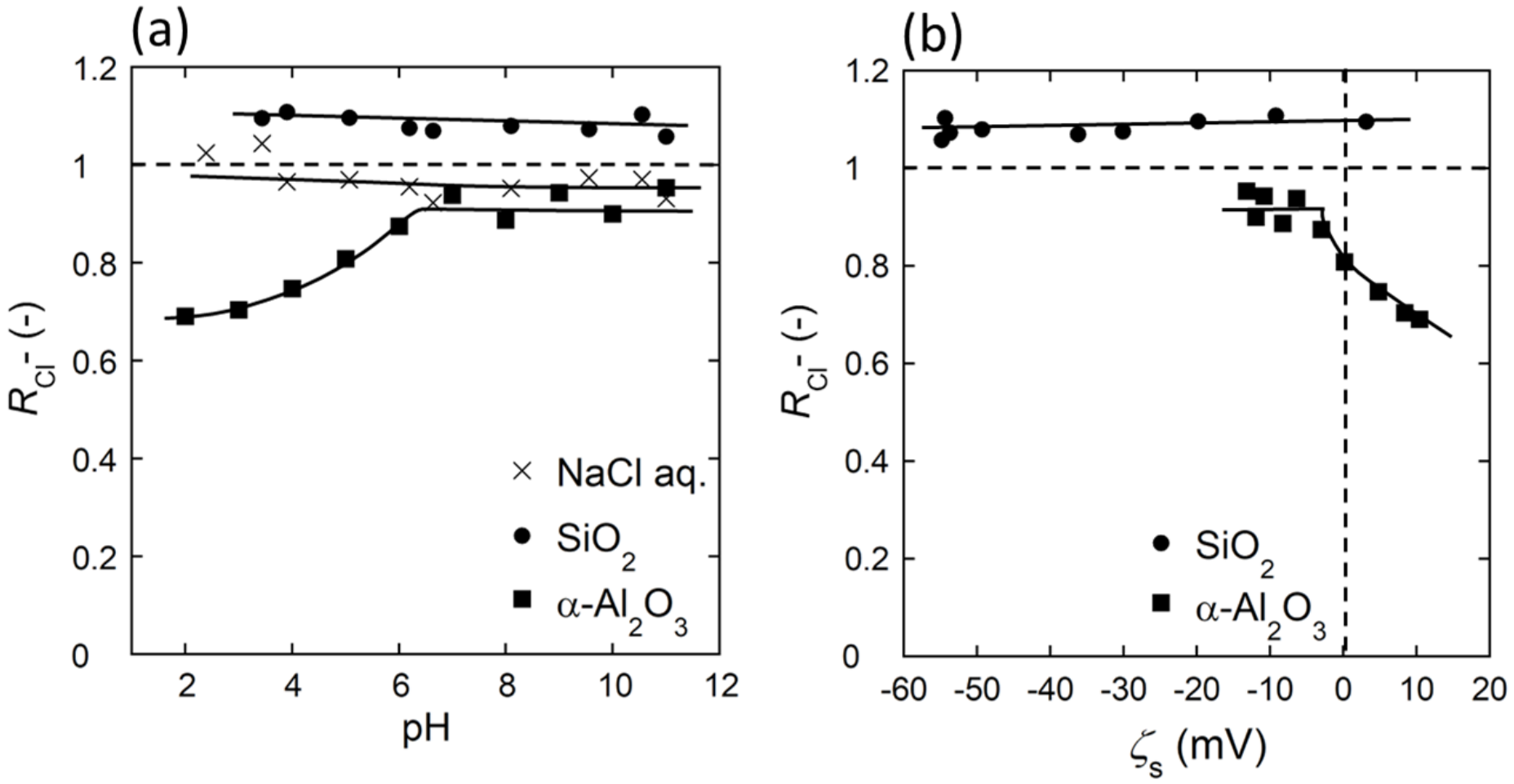

Figure 9. Dependences of the R_{Cl^-} on the pH (a) and the ζ_s (b) of 0.10 mol L^{-1} NaCl aq. with or without 10 vol% SiO_2 or α-Al_2O_3. The R_{Cl^-} are the detection rate which were calculated from the integrated intensities of the ^{35}Cl qNMR signal by eq 11.

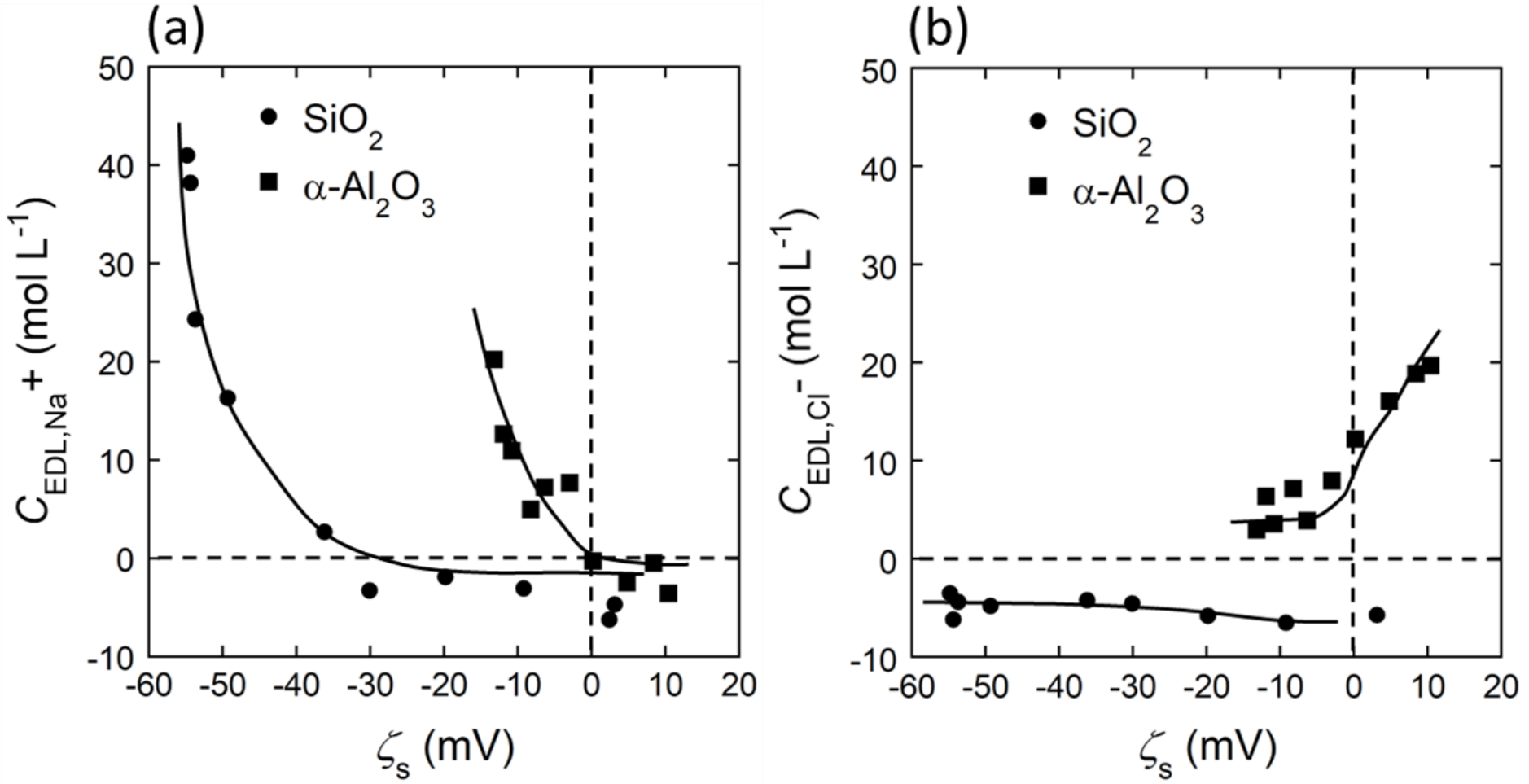

Figure 10 Dependences of the $C_{EDL,Na}$+ (a) and $C_{EDL,Cl}^-$ (b) on the ζ_s of 0.10 mol L^{-1} NaCl aq. with 10 vol% SiO_2 or α-Al_2O_3. The $C_{EDL,Na}$+ and $C_{EDL,Cl}^-$ are the apparent concentrations of Na^+ and Cl^- ions in an electric double layer (EDL) of a solid phase which were calculated from eq 14.

Colloids and Surfaces A:
Physicochemical and Engineering Aspects

Supplementary Material

Estimation of Solid-liquid Interfacial Potential Enabled by Quantitative Analysis and Relaxation Observation of Quadrupolar NMR

Hideshi Maki[a,b,*], Takashi Tachibana[c], Song Jung Eun[b] and Minoru Mizuhata[b,d]

[a]Center for Environmental Management, Kobe University, 1-1 Rokkodai-cho, Nada-ku, Kobe 657-8501, Japan

[b]Department of Chemical Science and Engineering, Graduate School of Engineering, Kobe University, 1-1 Rokkodai-cho, Nada-ku, Kobe 657-8501, Japan

[c]Department of Chemical Science and Engineering, Faculty of Engineering, Kobe University, 1-1 Rokkodai-cho, Nada-ku, Kobe 657-8501, Japan

[d]Faculty of Chemistry, Jagiellonian University, Gronostajowa 2, 30-387 Kraków, Poland

*Corresponding author: maki@kobe-u.ac.jp

Table S1. Physical properties of SiO_2 (KE-P50, NIPPON SHOKUBAI Co., Ltd., Japan) and α-Al_2O_3 (UA-5035, Showa Denko K.K., Japan) powder.

	Average primary particle diameter (nm)	Density, ρ_S (g cm^{-3})	Specific surface area, S_W (m^2 g^{-1})
SiO_2 (KE-P50)	500	2.22	6.8
α-Al_2O_3 (UA-5035)	500	4.03	3.5

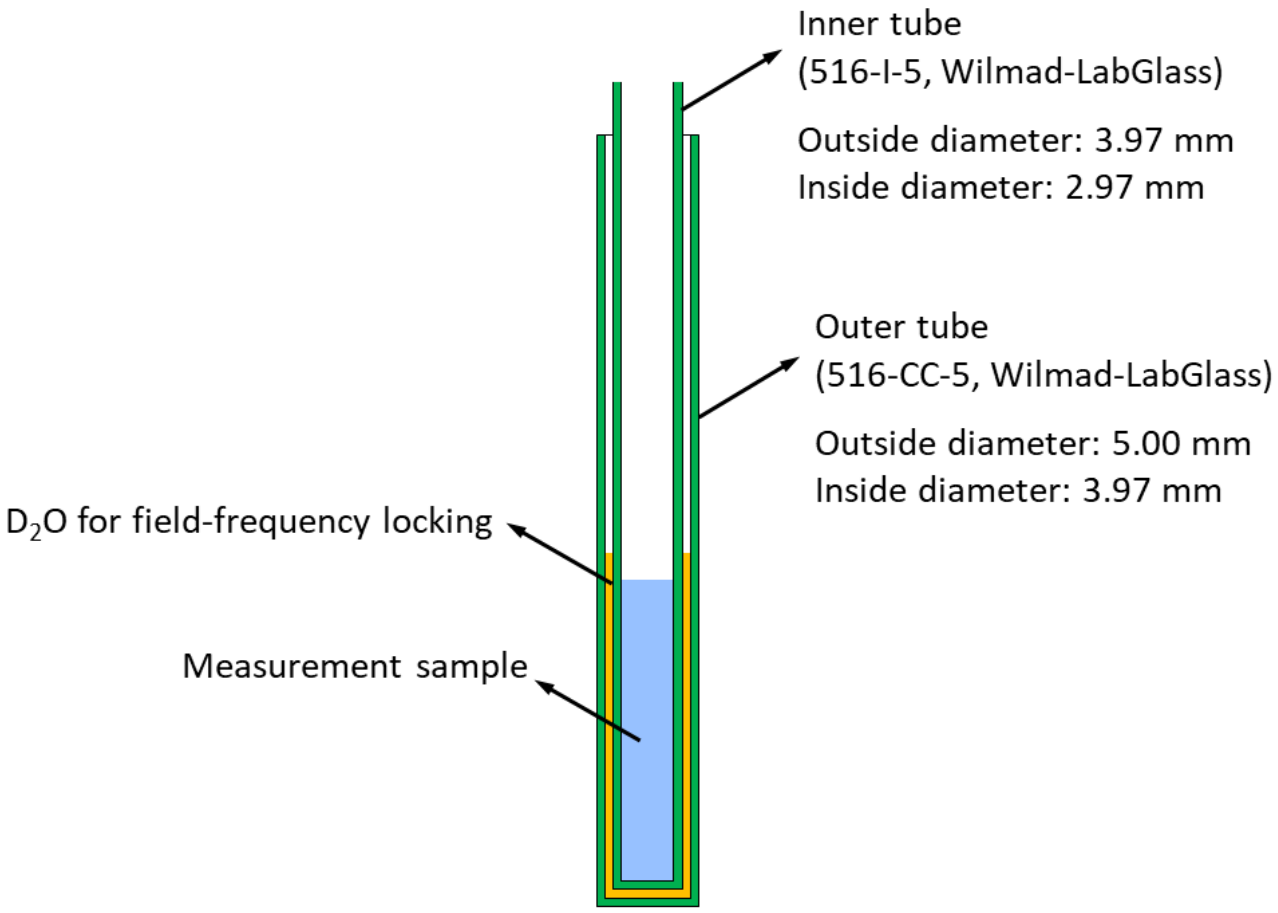

Scheme S1. Coaxial NMR tube system to avoid the contamination of D_2O for field-frequency locking into the measurement samples.

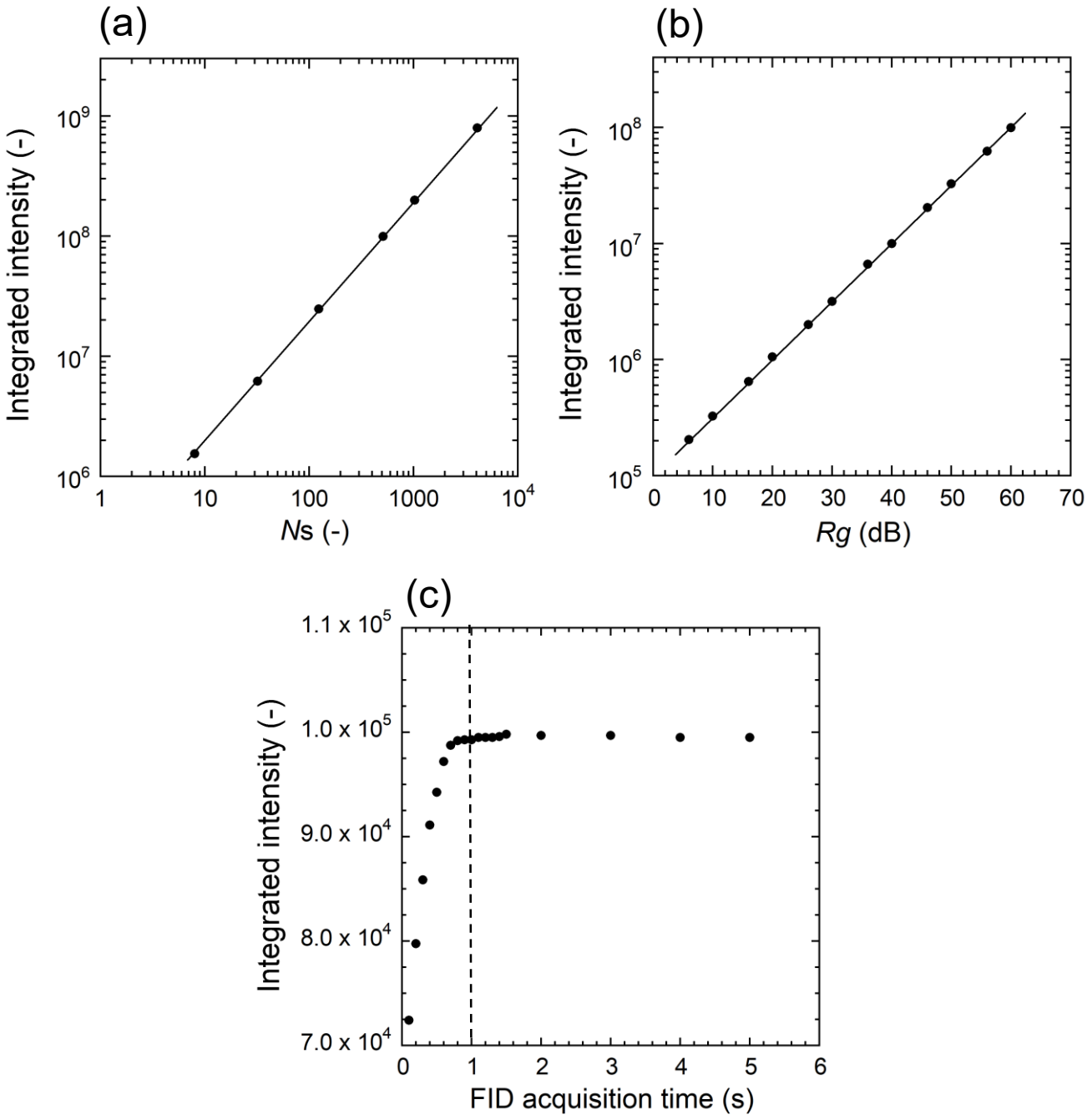

Fig. S1. NMR measurement parameter dependence of the integrated intensities of ^{23}Na NMR signals due to free Na^+ ion in 1 mol L^{-1} NaCl aq. at 20 ± 0.5 ˚C. NMR measurement parameter: (a) number of FID scans, *N*s, (b) receiver gain of a RF amplifier, *Rg*, and (c) FID acquisition time. The integrated intensities for (b) and (c) are the values per FID scan, and for (a) and (c) are converted into the values before the input into the RF amplifier in an NMR spectrometer (i.e., *Rg* = 0 dB).

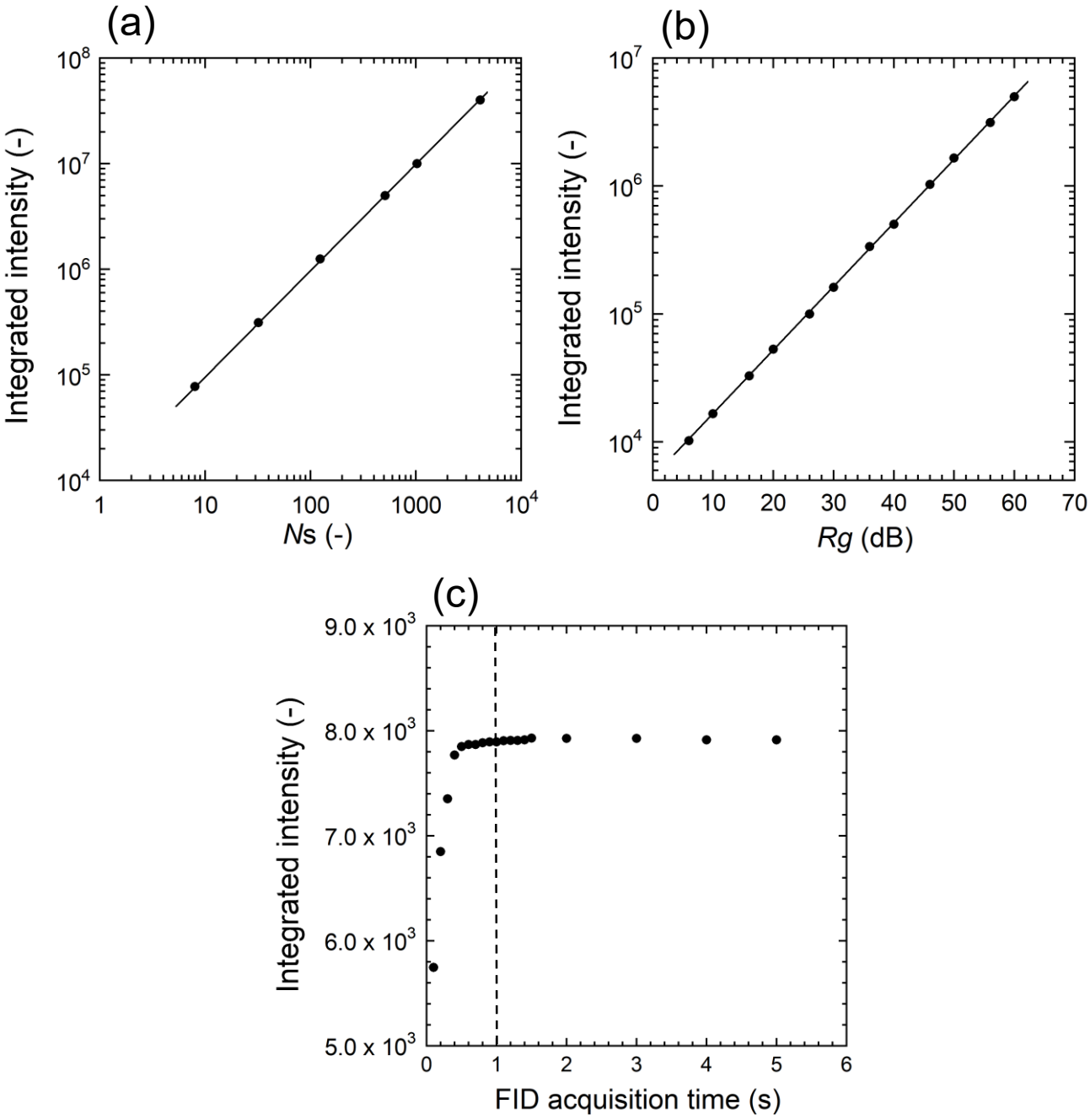

Fig. S2. NMR measurement parameter dependence of the integrated intensities of ^{35}Cl NMR signals due to free Cl^- ion in 1 mol L^{-1} NaCl aq. at 20 ± 0.5 ˚C. NMR measurement parameter: (a) number of FID scans, *N*s, (b) receiver gain of a RF amplifier, *Rg*, and (c) FID acquisition time. The integrated intensities for (b) and (c) are the values per FID scan, and for (a) and (c) are converted into the values before the input into the RF amplifier in an NMR spectrometer (i.e., *Rg* = 0 dB).

Table S2. All raw data for the relationships between the integrated intensities per FID scan (I_{freeNa}) of ^{23}Na NMR signals due to free Na^+ ion in x molL^{-1} NaCl aq. (x = ca. 1×10^{-3} – 2 mol L^{-1}) at 20 °C and the Na^+ ion concentrations (C_{freeNa}) as shown in Figs. 1(a) and 1(b). The I_{freeNa} values are converted into the values before the input into the RF amplifier in an NMR spectrometer (i.e., corresponding to Rg = 0 dB).

C_{freeNa} (mmolL^{-1})	I_{freeNa}	log (C_{freeNa}) (mmolL^{-1})	log (I_{freeNa})
0.400	1.2514×10^2	$^{-}$0.3979	2.097
0.600	1.8100×10^2	$^{-}$0.2219	2.258
1.000	2.928×10^2	0.0000	2.467
2.000	6.076×10^2	0.3010	2.784
4.000	1.1441×10^3	0.6021	3.059
6.000	1.9580×10^3	0.7782	3.292
8.000	2.575×10^3	0.9031	3.411
10.000	2.911×10^3	1.0000	3.464
20.00	6.292×10^3	1.3010	3.799
40.00	1.2367×10^4	1.6021	4.092
60.00	1.9053×10^4	1.7782	4.280
80.00	2.574×10^4	1.9031	4.411
100.00	3.217×10^4	2.000	4.507
200.0	6.224×10^4	2.301	4.794
400.0	1.2698×10^5	2.602	5.104
600.0	1.8334×10^5	2.778	5.263
800.0	2.476×10^5	2.903	5.394
1000.0	3.096×10^5	3.000	5.491
1200.0	3.788×10^5	3.079	5.578
1400.0	4.283×10^5	3.146	5.632
1600.0	4.890×10^5	3.204	5.689
2000	5.863×10^5	3.301	5.768

Table S3. All raw data for the relationships between the integrated intensities per FID scan (I_{freeCl}) of ^{35}Cl NMR signals due to free Cl^- ion in x molL^{-1} NaCl aq. (x = ca. 1×10^{-3} – 2 mol L^{-1}) at 20 °C and the Cl^- ion concentrations (C_{freeCl}) as shown in Figs. 2(a) and 1(b). The I_{freeCl} values are converted into the values before the input into the RF amplifier in an NMR spectrometer (i.e., corresponding to Rg = 0 dB).

C_{freeCl} (mmolL^{-1})	I_{freeCl}	log (C_{freeCl}) (mmolL^{-1})	log (I_{freeCl})
0.400	5.505×10^0	$^-$0.3979	0.7408
0.600	8.152×10^0	$^-$0.2219	0.9113
1.000	1.4896×10^1	0.0000	1.1731
2.000	2.979×10^1	0.3010	1.4741
4.000	5.515×10^1	0.6021	1.7416
6.000	8.141×10^1	0.7782	1.9107
8.000	1.0906×10^2	0.9031	2.038
10.000	1.3015×10^2	1.0000	2.114
20.00	2.809×10^2	1.3010	2.449
40.00	5.726×10^2	1.6021	2.758
60.00	8.268×10^2	1.7782	2.917
80.00	1.1219×10^3	1.9031	3.050
100.00	1.4116×10^3	2.000	3.150
200.0	2.808×10^3	2.301	3.448
400.0	5.681×10^3	2.602	3.754
600.0	8.536×10^3	2.778	3.931
800.0	1.1455×10^4	2.903	4.059
1000.0	1.4207×10^4	3.000	4.153
1200.0	1.6899×10^4	3.079	4.228
1400.0	1.9888×10^4	3.146	4.299
1600.0	2.314×10^4	3.204	4.364
2000	2.905×10^4	3.301	4.463

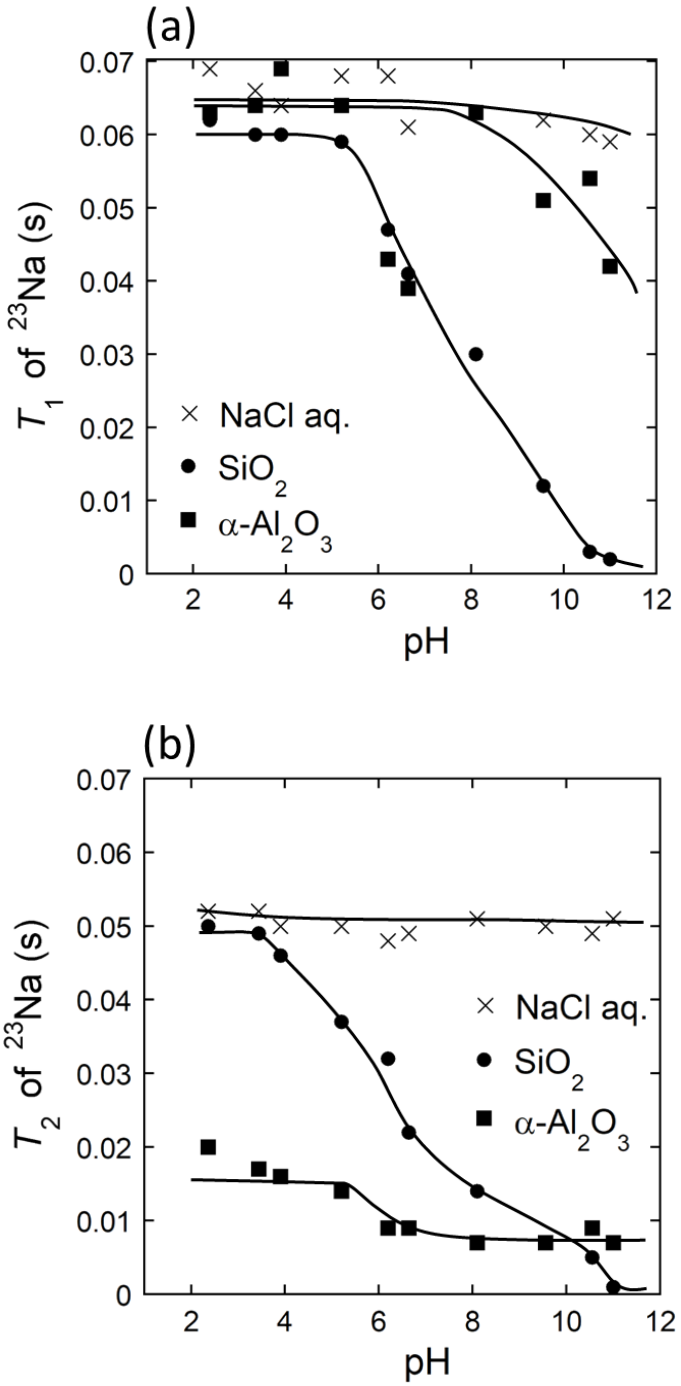

Fig. S3. Dependence of the T_1 (a) and the T_2 (b) of ^{23}Na NMR on the pH of 0.10 mol L^{-1} NaCl aq. with or without 10 vol% SiO_2 or α-Al_2O_3.

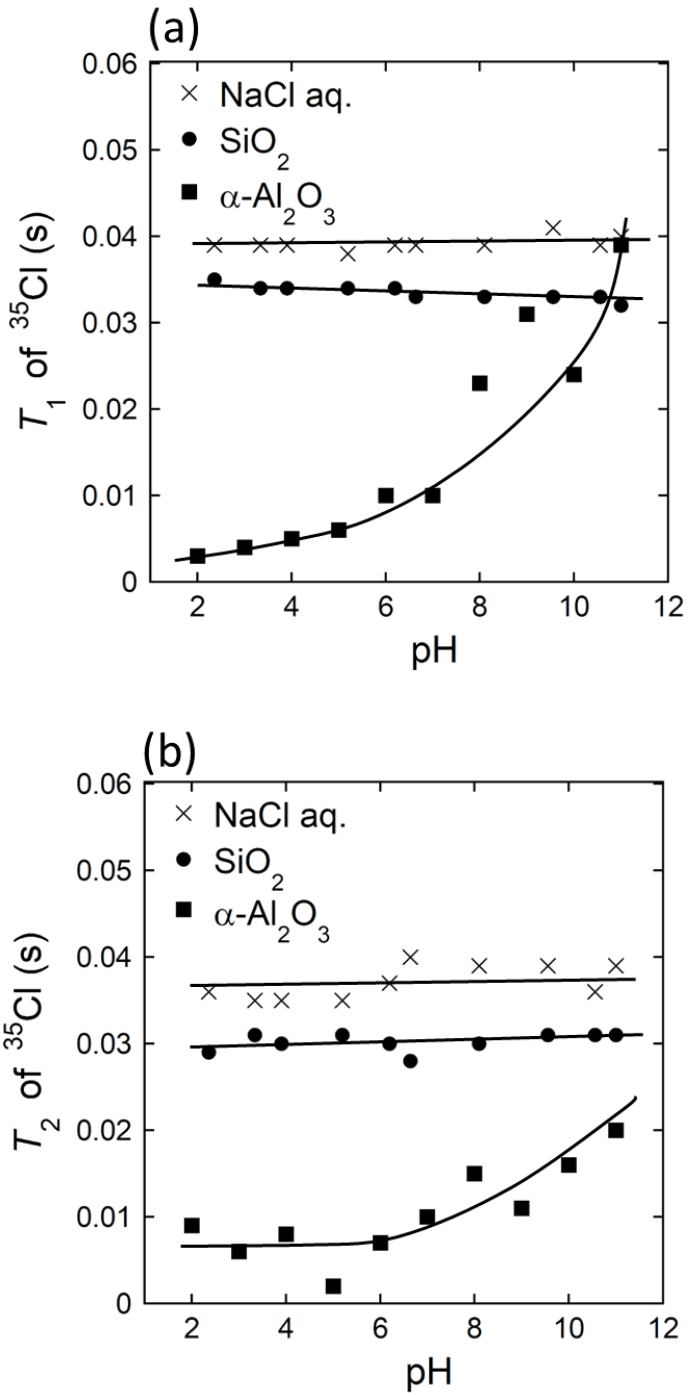

Fig. S4. Dependence of the T_1 (a) and the T_2 (b) of ^{35}Cl NMR on the pH of 0.10 mol L^{-1} NaCl aq. with or without 10 vol% SiO_2 or α-Al_2O_3.